POLITECNICO DI TORINO

Master's Degree in Energy and Nuclear Engineering

Politecnico
di Torino

Master's Degree Thesis

The design and manufacturing of the cathode air compression and treatment system for a test bench of direct methanol fuel cells.

Supervisors

Prof. Massimo SANTARELLI

Prof. Teresa LEO MENA

Prof. Rafael D'AMORE-DOMENECH

Candidate

Gaia LOMBARDI

July 2024

Abstract

The growing concern about climate change and the energy crisis has driven the development of technologies aimed at reducing environmental impacts, such as renewable energy sources and the use of energy carriers like hydrogen or methanol in fuel cells. Fuel cells are electrochemical devices that convert chemical energy from fuels into electrical energy and heat with high efficiency. Despite their wide recognition, several technological challenges remain, hindering their extensive use.

To improve fuel cell technology, specialised test benches are used to control and monitor critical operating conditions, such as fuel supply, air flow, temperature, and humidity. This thesis introduces a new air treatment system for a fuel cell test bench, enabling precise control of air temperature, humidity, and flow rate.

Accurate control of these air properties is essential for studying fuel cell performance under conditions similar to those in the real world. By managing the inlet air parameters, it is possible to gain deeper insights into fuel cell behaviour and identify ways to improve efficiency, durability, and cost-effectiveness.

Using psychrometric principles and equations, the feasibility of the studied configuration is analysed to achieve the desired temperature and humidity conditions required by the fuel cell, given the starting conditions in the laboratory environment.

The findings of this thesis offer a novel approach to the design of air treatment systems for fuel cell test benches, addressing a critical gap in the integration of renewable energy technologies. The insights gained from this research can support the ongoing development and optimisation of fuel cell systems, ultimately aiding the transition towards a sustainable energy future.

Table of Contents

List of Tables

List of Figures

Acronyms

DMFC
Direct Methanol Fuel Cell

DMFC
Proton Exchange Membrane Fuel Cell

AFC
Alkaline Fuel Cell

PAFC
Phosphoric Acid Fuel Cell

SOFC
Solid Oxide Fuel Cell

MCFC
Molten Carbonate Fuel Cell

OCV
Open Circuit Voltage

CCUS
Carbon Capture and Storage

MEA
Membrane Electrolyte Assembly

PEM
Polymer Electrolyte Membrane

PTEF

Polytetrafluoroethylene

S-PEEK

Sulfonated PolyEtherEtherKetone

PBI

Polybenzimidazole Acid

FEC

Flowing Electrode Channe

ORR

Oxygen reduction reaction

Pt

Platinum

Tu

Ruthenium

GDL

Gas Diffusion Layer

BP

Bipolar Plate

PP

polypropylene

PPS

polyphenylene sulphide

PVDF

polyvinylidene fluoride

ICR

interfacial contact resistance

CEGR

Cathode Exhaust Gas Recirculatione

PID

Proportional–integral–derivative controller

PTFE

polytetrafluoroethylenee

RH

Relative Humidity

Chapter 1

Introduction

As countries become more industrialised by the decade, energy becomes increasingly vital to society, leading to a significant surge in demand [1]. Nowadays the entire world is facing a climate crisis due to the huge amount of emissions coming from different sectors, including energy production, transportation, and industry, among others [2]. The main culprit driving this crisis is fossil fuel, a finite and polluting resource that releases greenhouse gases into the atmosphere [3]. The improvement in the standard of living in industrialised nations necessitates greater energy consumption, leading to a heightened reliance on fossil fuels. The transport sector, which is the sector with the highest reliance on fossil fuel [2], is the second most pollutant sector, after the power industry, representing 20.7 % in 2022 [4], as it can seen in the figure 1.1.

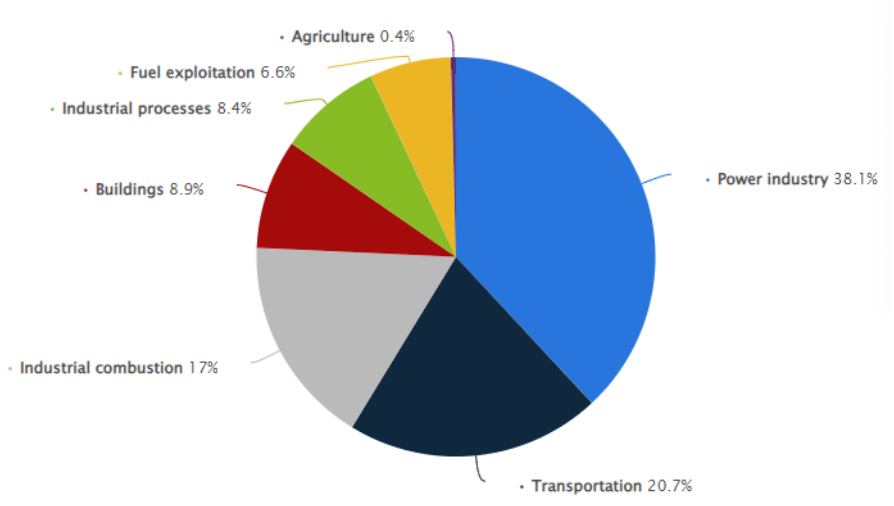

Figure 1.1: Emission by Sector. [4]

The world is mobilising to find a solution to climate change and global warming. A viable alternative to fossil fuels is renewable energy. However, this technology has a significant drawback represented by their dependence on the weather and daylight, leading to variability in energy production from sources such as the sun and wind, which are not constant throughout a period [5].

To address this challenge, researchers have been exploring various methods to store renewable energy efficiently. One promising approach is to convert surplus renewable energy into fuels that can be stored for long periods and later converted back into electrical energy. This concept, often referred to "power-to-X," is particularly relevant for seasonal storage, where large amounts of energy produced during periods of high production need to be stored to ensure a consistent supply during periods of low production [6].

Among the most efficient ways of converting fuel back into electrical energy is through a fuel cell, which is explained in the next section of this chapter. They offer several advantages over traditional energy storage methods, including high efficiency, low emissions, and quiet operation.

In the context of renewable energy, fuel cells can be used to store energy generated from intermittent sources such as solar and wind power in the form of fuel. This stored energy can then be used to generate electricity when needed, ensuring a reliable and consistent supply. The use of fuel cells in this manner can significantly reduce the reliance on fossil fuels and help mitigate the variability associated with renewable energy sources.

This thesis focuses on a Direct Methanol Fuel Cell (DMFC), which is a type of fuel cell that uses methanol as the fuel. The DMFC is ambitious in its future applications, aiming to power airplanes and ships, thereby reducing emissions from the transportation sector. The development of such technology has the potential to revolutionise the way we generate and use energy, making it a crucial component in the fight against climate change.

1.1 Fuel Cell

Fuel cells [7] are electrochemical devices able to convert chemical energy into electrical energy. To better understand the concept of a fuel cell, it can be compared to a battery, look at figure 1.2: they are both electrochemical devices that produce energy, but the latter has a closed circuit, able to store the energy which degrades over time, while the former has an opened circuit, alimented with an external fuel, which has a much longer lifespan.

Different types of fuel cells have been developed, each with distinct characteristics, but they generally share a similar structure comprising an anode, an electrolyte, and a cathode. At the anode, where fuel is supplied, oxidation occurs, producing

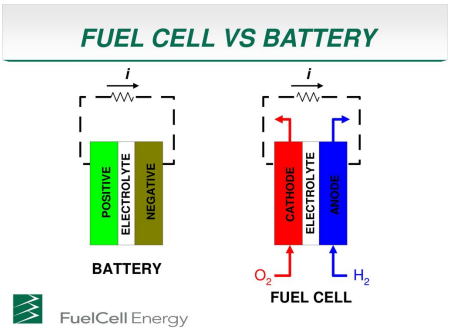

Figure 1.2: Fuel Cell vs Battery [8]

electrons and ions. The ions pass through the electrolyte - a membrane in direct contact with the electrodes that does not conduct electricity in the form of electrons - and reach the cathode. Simultaneously, electrons flow through an external circuit to the cathode, generating current. Typically, the cathode is supplied with oxygen and the reduction reactions take place. By accepting electrons from the anode, oxygen molecules split into oxygen atoms, reacting with the ions coming from the electrolyte.

One of the most well-known fuel cells is powered by hydrogen, depicted in Figure 1.3. In such a figure, the electrolyte is acidic as it features conductivity to protons.

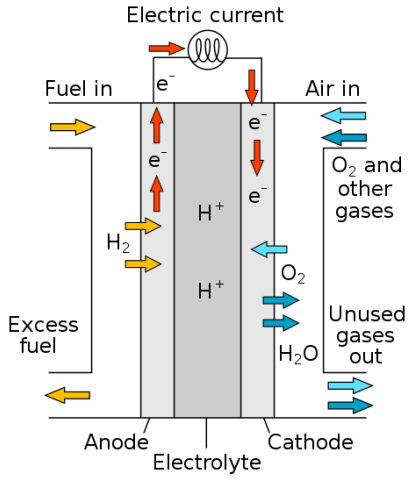

Figure 1.3: Hydrogen Fuel Cell

As mentioned, various types of fuel cells exist, primarily differing in the operating temperature and consequently, in the materials used.
Low-temperature fuel cells exhibit a dynamic behaviour with a rapid switch on/off,

finding the main applications in transportation devices. The main types are DMFC, Proton Exchange Membrane Fuel Cell, AFC, Alkaline Fuel Cell, DMFC, Direct Methanol Fuel Cell, and PAFC, Phosphoric Acid Fuel Cell. In contrast, the high-temperature ones are used for stationary applications due to their slower on/off time, with notable examples being SOFC, Solid Oxide Fuel Cell, and MCFC, Molten Carbonate Fuel Cell.
The table below 1.1 sums up the main characteristics [9]:

Table 1.1: Types of Fuel Cell

Fuel Cell Types	Typical Electrolyte	Operating temperature [°C]	Typical stack size [kW]	Electrical Efficiency [%]
PEMFC	Nafion	<120	1-100	40-60
AFC	KOH	<100	1-100	60
DMFC	Nafion	60-130	1-100	40
PAFC	H_3PO_4	150-200	5-400	40
SOFC	YSZ	500-1000	300-3000	60
MCFC	K_2CO_3 Ca_2CO_3	600-700	1-2000	50

The effects that result from the reactions within the fuel cell are twofold:

- Generation of electrons flow across the external circuit, resulting in current I circulation
- Generation of a voltage gradient ΔV across both the anode and cathode, creating a voltage gradient across the cell.

Combining these two effects the generation of the power W_{el} can be found:

$$W_{el} = V_{cell} \times I \tag{1.1}$$

Given that a single cell produces a low voltage, connecting multiple cells in series to form a stack is advisable to increase power output. Interconnectors or bipolar plates are used between the anodes and cathodes to link several fuel cells together. Generally composed of metallic material to enhance electrical conductivity, these components must be ion-insulated, and typically have a thickness of $1mm$.
The fuel cell ends on both edges with end plates, facilitating the insertion of fuel and air into the system. To minimize losses in the fuel cells, insulating materials are employed to prevent fuel leakage or unwanted air intake, positioned in contact with the end plates.

1.1.1 Thermodynamic analysis of a fuel cell

Beginning from a thermodynamic analysis, wherein reactants, products, heat flow, and electrical work are studied, the fundamental equation of the fuel cell, known as the Nernst Equation, can be derived [10]:

$$E = -\frac{\Delta g_{reaction}(T, p_0)}{z_f F} + \frac{R \cdot T}{z_f F} \cdot \ln\left(\frac{\prod^R \left(\frac{p_i}{p_0}\right)^v}{\prod^P \left(\frac{p_i}{p_0}\right)^v}\right) \tag{1.2}$$

Where p_0 is the reference pressure, p_i reference to the partial pressure of reactants in the numerator and products in the denominator; R is the ideal gas constant; T is the cell temperature; z_f is the charge number of the fuel; F is the Faraday constant; Δg is the Gibbs free-energy, $\Delta g < 0$ in fuel cell.
The variable E is the result of the reaction and the thermodynamic conditions. It represents the voltage gradient across the cell in open circuit condition OCV when there's no electrical connection and no transfer phenomenon occurs, therefore in an equilibrium condition. Closing the circuit the equilibrium disappears and the transfer phenomena generating the voltage gradient with respect to OCV emerge, termed overvoltage. The equation transforms as follows:

$$V_{cell}(i) = E - \eta_{act} - \eta_{ohm} - \eta_{diff} \tag{1.3}$$

- η_{act}: is the activation overvoltage and it is related to the charge transfer at the electrode, due to the kinetic of reactions;

- η_{ohm}: is the ohmic overvoltage, related to the charge migration of the electrons and the ions, mainly due to the resistance of the different components;

- η_{diff}: is the diffusion overvoltage, related to the mass transport, due to the molecular diffusion inside the electrodes.

Through these phenomena, it is possible to draw the polarization curve shown in Figure 1.4, a fundamental tool for describing the performance of a fuel cell that shows the relationship between the cell voltage and the current density:

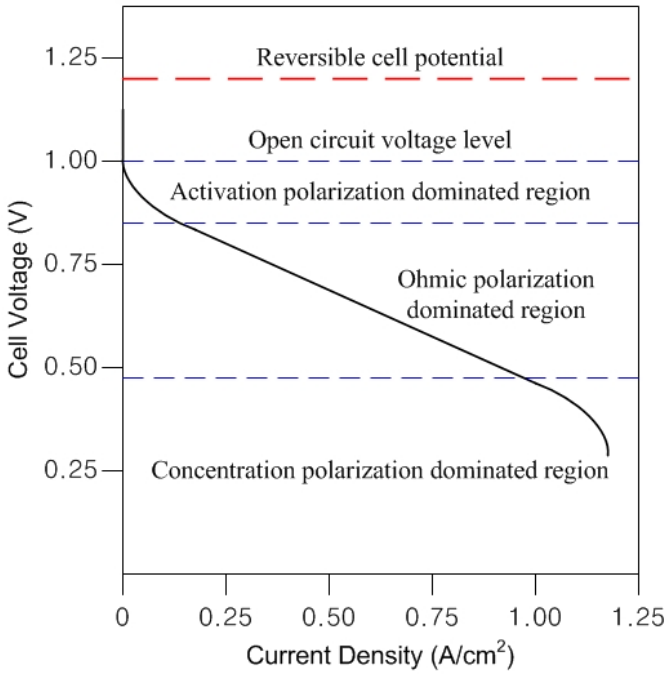

Figure 1.4: Polarization Curve [11]

1.2 Methanol

Methanol, with the chemical formula CH_3OH, is an organic compound also known as methyl alcohol. It is a colourless liquid, flammable and has a characteristic slightly sweet smell. One of its main characteristics is its versatility as a chemical fuel. In fact, methanol is a clean-burning, low-carbon fuel that is becoming increasingly popular in the marine industry. Methanol has the highest hydrogen-to-carbon ratio of any liquid fuel at ambient conditions and it can be stored as a liquid at ambient temperature and pressure, making it an important energy carrier and alternative fuel. The majority of fuel cells today are powered by hydrogen. The choice of methanol over hydrogen is due to its advantages in storage, transport and use. In fact, hydrogen has many problems related to the specific work required to liquefy it, as it liquefies at -253°C, a special bulky pressure tank is required to store and transport it, in order to avoid the embrittlement, and the pipe distribution system is not ready to be filled with hydrogen. Methanol, on the other hand, is liquid at ambient conditions, it is easy to store and transport, and the infrastructure for methanol is already partly in place due to its use as a conventional fuel. Moreover, hydrogen poses safety issues as it is highly flammable and requires additional precautions to ensure safety during handling, storage, and usage. Methanol, on the other hand, is less volatile and presents lower safety risks compared to hydrogen.

Hydrogen requires a production process that often involves water electrolysis or methane reforming, both of which require energy. This can reduce the overall efficiency of the fuel cell system compared to the direct use of methanol, which can be more easily obtained from renewable sources or less energy-intensive feedstocks.

Methanol Production

There are different categories of methanol based on the production process and the source of raw material used [12]:

- **Grey methanol**: This is the most common category of methanol, which is derived from fossil fuels like natural gas, coal, or petroleum. The production process involves converting these raw materials into synthesis gas (syngas), which is then transformed into methanol through a catalytic process.
- **Blue methanol**: Produced from a process that uses Carbon Capture and Storage (CCUS). The resulting product of this process is considered blue methanol and would have significantly lower emissions than conventional methanol.
- **E-Methanol**: Created utilizing green hydrogen, which is hydrogen produced via renewable electricity sources. When combined with CO2 captured from renewable sources like bioenergy with carbon capture and Direct Air Capture, it yields what is known as green methanol.
- **Bio-Methanol**: Derived from renewable natural gas obtained from sources such as landfills, sewage plants, or animal manure farms. It can also be produced from biomass feedstock, which may include sustainable sources like forestry and agricultural waste by-products, municipal solid waste, and black liquor from the pulp and paper industry. The production process involves converting biomass into synthesis gas (syngas) through gasification, which is then converted into methanol through a catalytic process.

Although methanol might be produced in a more environmentally sustainable manner compared to hydrogen, it still faces significant economic challenges.

1.3 Thesis structure

In this Master Thesis, a Direct Methanol Fuel Cell is examined, focusing on the air circuit entering the cell and on the electrical regulation of the devices regulating the circuit. The structure of the thesis is as follows:

- In Chapter 1 an introduction of the work is provided, starting to focus on fuel cells and their operation, this includes a discussion on the different types of fuel cells and a thermodynamic analysis of their operation. Additionally, the chapter introduces methanol as a fuel source, highlighting its production process and comparing its characteristics to hydrogen
- Chapter 2 provides information about the state-of-the-art technologies related to direct methanol fuel cells (DMFCs), describing their structure and the material utilized in literature for the different parts of the cell. Furthermore, the chapter explores existing literature on air treatment systems, providing insights into their design and functionality
- Moving forward, Chapter 3 focuses on the design requirements, this includes defining operational parameters such as mass flow rate, temperature, and humidity, along with the associated calculations.
- In Chapter 4, the concept engineering behind the chosen circuit design is elucidated, clarifying the rationale behind the specific configuration and material selection.
- Chapter 5 introduces the modelling aspects of the project, containing both thermodynamic modelling and the implementation of a Proportional Integral Derivative (PID) controller within the electrical circuit.
- Chapter 6 explains the basic and detailed engineering, detailing the development of a piping and instrumentation diagram (P&ID) and specifying the characteristics of individual system components.
- Chapter 7 shifts focus towards the fabrication process, detailing the assembly of the system, showcasing the final product, and addressing any encountered challenges and their respective solutions.
- Finally, Chapter 8 tells the conclusion of this project.

Chapter 2

State of the art

2.1 Direct Methanol Fuel Cell

As mentioned above, the subject of this thesis is the DMFC. This is a fuel cell working at low temperatures, according to Table 1.1. The particular advantage of this technology lies in the fuel itself, which is a liquid fuel at ambient conditions. Methanol is an attractive fuel compared to hydrogen for different reasons [13]:

- Being in liquid form gives it a higher specific energy density, avoiding all the storage problems of hydrogen, which requires a huge amount of energy to be compressed or liquefied.
- It is perceived to be a safer fuel since the hydrogen is highly flammable.
- The infrastructures needed for the development of a hydrogen economy are not economic, while for the methanol the existing ones are already suitable.
- The production is more sustainable since it can be produced from biomass and recycled carbon dioxide (CO_2).
- Another attractive advantage of methanol is that it is fed directly to the anode, eliminating the need for a fuel reformer, and saving space and energy.

The structure of the DMFC is the same as that described in the previous chapter: it has an anode, an electrolyte, and a cathode. Through Figure 2.1, it is possible to see a schematic operation of the fuel cell:

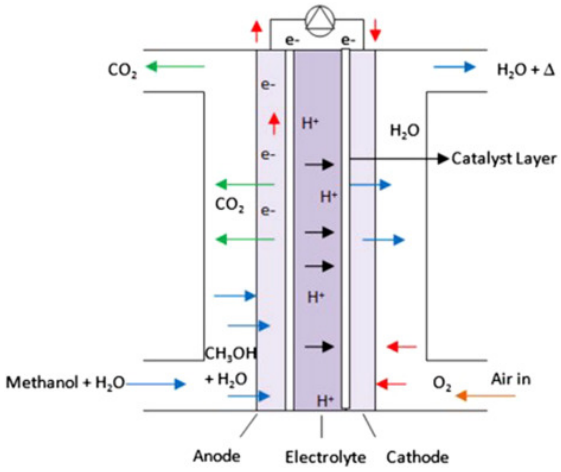

Figure 2.1: Direct Methanol Fuel Cell [14]

As can be seen from the figure above, methanol is fed into the anode diluted in a water solution in a concentration of $1M$. The reaction of methanol and water produced: carbon dioxide CO_2, which is expelled from the fuel cell, protons of hydrogen, which flow in the cathode through the electrolyte, and electrons, which flow in the cathode through the external circuit.

The anode reaction is an oxidation reaction:

$$CH_3OH + H_2O \longrightarrow CO_2 + 6\,H^+ + 6\,e^- \quad (E_{anode} = 0.03V) \tag{2.1}$$

The cathode is fed directly with air. This brings an innovation to the fuel cell under investigation, with a particular advantage: the direct supply of ambient air eliminates the need for an oxygen tank. The reaction on the cathode side does not differ from that of a normal fuel cell, and what will react is only the oxygen O_2. Nitrogen N_2, argon Ar, and carbon dioxide CO_2 are inert gases simply expelled from the cathode side. O_2 will react with the products sent from the anode: hydrogen protons and electrons.

The cathode reaction is a reduction reaction:

$$\frac{3}{2}\,O_2 + 6\,H^+ + 6\,e^- \longrightarrow 3\,H_2O \quad (E_{cathode} = 1.24V) \tag{2.2}$$

The overall reaction of this fuel cell is:

$$CH_3OH + \frac{3}{2}\,O_2 \longrightarrow CO_2 + 2\,H_2O \quad (E_{cell} = 1.21V) \tag{2.3}$$

As discussed in the previous chapter, the value of the effective potential of the fuel cell is not the one written above, but it is affected by the overvoltage.

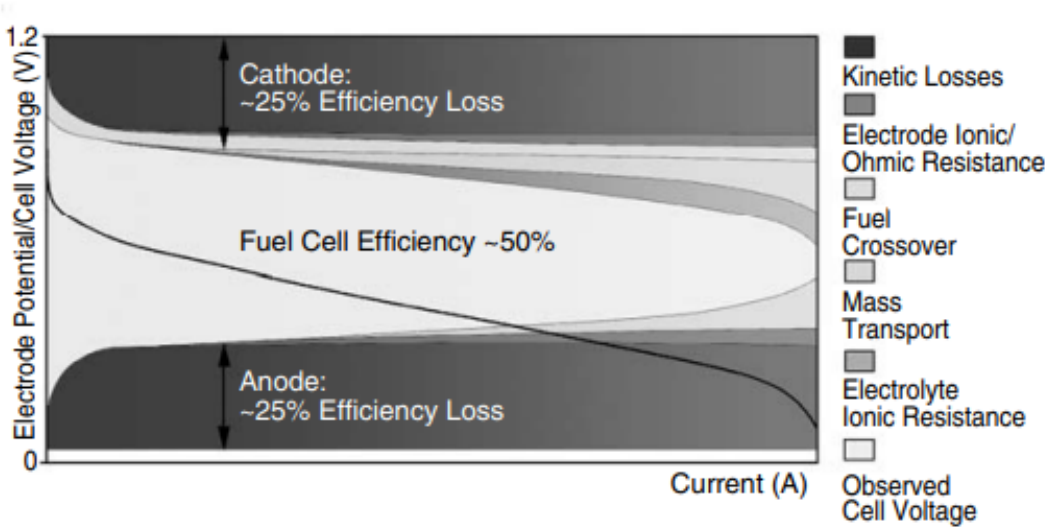

Figure 2.2: Polarization curve of DMFC [15]

In particular, looking at figure 2.2, the most significant hindering factor is the activation overvoltage, which restricts the rate of the electrode reactions, decreasing the cell voltage up to 400-600 mV, also affecting the voltage efficiency, reducing it to 50%. In the paragraph 2.1.1.2 these issues are explained.

The general structure of a DMFC is shown in the figure above 2.3:

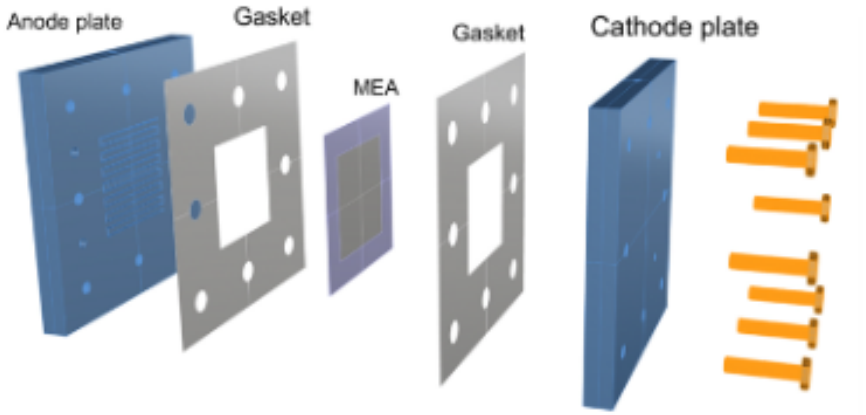

Figure 2.3: Exploted structure of DFMC

In the next paragraphs, each layer of the DMFC is explained.

2.1.1 Membrane Electrolyte Assembly

The heart of the entire fuel cell is the Membrane Electrolyte Assembly (MEA), which converts the methanol directly into electricity through the previous electrochemical reactions. It comprises the Polymer Electrolyte Membrane (PEM), the actual electrolyte, two electrodes (cathode and anode), and catalyst systems.

2.1.1.1 PEM

In the literature, it is possible to see that the most widely used material as PEM is Nafion, a composed material made starting from a hydrophobic polytetrafluoroethylene (PTFE) backbone and a hydrophilic perfluorinated vinyl ether pendant side chain, as it is possible to see in the figure 2.4. The side chain is ionically bonded to a sulfonic acid group ($-SO_3H$), in which the negatively charged SO_3- groups block anions while allowing cations to pass through. The hydrophilic nature of Nafion aids in water absorption, maintaining membrane hydration and assisting proton migration. Water absorption by sulfonic acid groups forms hydrophilic ion-cluster domains and water bridges, serving as proton migration channels and enhancing proton transfer [16]. Nafion membranes exhibit proton conductivity exclusively when water is present, and the efficiency of proton conduction diminishes as the membrane's hydration level decreases. Consequently, DMFCs utilizing acid membranes usually function within a humidity of 100% and a temperature range of 50°C to 90°C, representing a compromise between competing factors. Raising the temperature would enhance performance due to improved water management, more efficient reaction rates, increased tolerance to carbon monoxide by the anode electrocatalyst, faster heat dissipation, and enhanced integration within the system [17].

PEM is designed to perform multiple functions at the same time [16]:

1. High proton conductivity:
    - Essential for preventing ohmic loss and supporting high current densities in DMFCs.
    - Proton-conducting functionalities (sulfonic acid) within polymer chains facilitate the formation of ionic clusters for effective proton migration.
    - External factors like temperature and relative humidity affect proton conductivity, and water content in the membrane plays a crucial role.
2. Low methanol permeability:
    - Crucial for minimizing methanol crossover, better explained in next chapters, which can waste fuel, reduce efficiency, and negatively impact DMFC performance and durability.

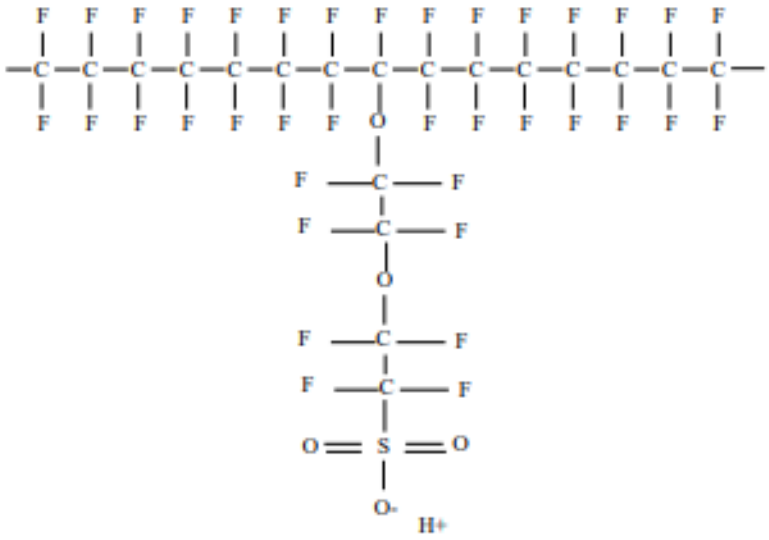

Figure 2.4: Nafion Molecule [7]

- Methanol permeability increases with temperature and concentration but decreases with higher current density.
- The alignment, orientation, and local packing density of the membrane matrix influence methanol permeability.

3. High electrical resistivity:

   - PEMs should reject electron transport, ensuring electrons are driven to an external circuit for electricity generation.
   - Maintaining a balance between proton and electron transport is crucial for overall cell efficiency.

4. Suitable chemical stability:

   - Chemical durability is essential for the membrane's longevity, given the anode's oxidising environment and the cathode's reducing environment.
   - Radical degradation, caused by intermediate products like hydroxyl radicals, can lead to defragmentation and thinning of the membrane.

- Stability improvements can be achieved through short side-chain polymers, hydrocarbon polymer electrolyte modifications, and methods to mitigate free radical degradation.

5. Suitable mechanical stability:

   - Mechanical strength is critical to withstand dimensional changes during fuel cell operation, preventing cracks and pinholes.
   - The flexibility and low rigidity of the membrane are crucial for enduring mechanical stresses and preventing damage.
   - Carbon nanomaterials are utilized as reinforcing agents to enhance mechanical stability.

Penalising factors

1. **Methanol crossover**

   The methanol crossover is the undesired phenomenon of diffusion of the methanol molecule from the anode to the cathode, through the PEM. Once the methanol reaches the cathode, it may react with oxygen, causing the cathode potential to drop. The methanol crossover is pushed by water, which provides the proton conductivity pathway in acid membranes, due to the ability to absorb methanol readily. Such action reduces the open-circuit voltage of the cell which, in turn, adversely affects the performance of the fuel cell at all currents [18]. Studies bring to an evaluation of the influence of different operating parameters [19]:

   - Influence of methanol concentration: an increase in methanol concentration in the anode feed is associated with a decrease in open-circuit voltages, likely due to a higher transport rate through the membrane. For this reason, the methanol concentration is strictly below 5 M and is typically 1 M. A second advantage of a dilute methanol solution is that water is in contact with the MEA and thus ensures that the membrane is hydrated, which is, of course, important for acid membranes. However, at low methanol concentrations, a reduction in cell performance is observed, attributed to concentration polarization effects.
   - Influence of pressure: Increasing oxygen/air pressure significantly impacts cell performance, reducing methanol crossover, and resulting in higher cell voltages.
   - Influence of temperature: Increasing temperature improves cell performance, despite the increase in methanol crossover.

- Influence of membrane thickness and equivalent weight: methanol crossover decreases with increasing membrane thickness, but this trend changes at higher current densities. The membrane's equivalent weight influences cell performance, with high equivalent weight membranes showing lower methanol permeability.

In order to decrease the methanol crossover several solutions could be applied: a thick PEM electrolyte should be used. These will bring also an increase in cell resistance. For a DMFC, the membrane normally has a thickness of between 0.15 and 0.20 mm compared with between 0.05 and 0.10 mm for a hydrogen PEMFC.

In the DMFC's case study, the PEM utilized is Nafion 117 with a thickness of 0.187 mm.

Certainly, the platinum material used for the catalyst is a reason why the crossover is so elevating, so substituting this material could be another option.

2. **Water management**

   Another problem associated with the membrane, and more generally with the DMFC, is water management. As mentioned above, maintaining a certain level of water in the fuel cell is essential to hydrate the membrane and allow high proton conductivity. The ideal operation should be a constant hydration due to the formation of water on the cathode side, while the air blowing in dries the excess water. However, under operating conditions, when the hydrogen passes through the electrolyte from the anode to the cathode side, the water molecules follow the same path, leaving the anode dry. For this reason, it is essential to dilute the methanol in water and to humidify the air. Nevertheless, it may occur flooding of the positive electrode due to an excess of water; the water that is not properly removed, significantly hinders the transport of oxygen to the active sites of the electrode, destabilizing the cell's operation and simultaneously affecting its performance.

Alternative to Nafion

Various solutions are being studied in the market to find an alternative to Nafion. In addition to the disadvantages mentioned above, Nafion has the negative aspects of increasing cost and low operating temperature. Working at a higher temperature brings advantages in terms of the speed of reactions, increasing the efficiency of the whole cell.

The two most promising alternatives are Sulfonated PolyEtherEtherKetone (S-PEEK) and Polybenzimidazole Acid (PBI) membranes [20]. S-PEEK offers a lower cost compared to Nafion, improved thermal and chemical stability, and mechanical

resistance. However, it has slightly lower proton conductivity than Nafion, which can be enhanced through post-sulfonation. Increasing post-sulfonation, though, leads to decreased mechanical stability and higher sensitivity to dehydration. The membrane exhibits significant swelling at high temperatures and humidity. On the other hand, PBI demonstrates good chemical and thermal stability, low methanol crossover, and the ability to operate at higher temperatures, enhancing reaction kinetics and reducing catalyst poisoning. Challenges include lower proton conductivity compared to Nafion and difficulties in processing.

Alternative to PEM

Two main electrolytes are analysed as alternatives to PEM:

- **Flowing Electrolyte**

  A Direct Methanol Fuel Cell that uses this type of electrolyte is called Flowing Electrolyte-Direct Methanol Fuel Cell (FE-DMFC) [21]. This electrolyte uses a fluid capable of conducting ions, a sulfuric acid solution (H_2SO_4), allowing protons to be transferred from the anode to the cathode. This fluid passes through a porous material, effectively removing any methanol that has crossed from one side of the cell to the other. A schematic of this fuel cell is shown in Figure 2.5, showing also the chemical reactions which occur on it.

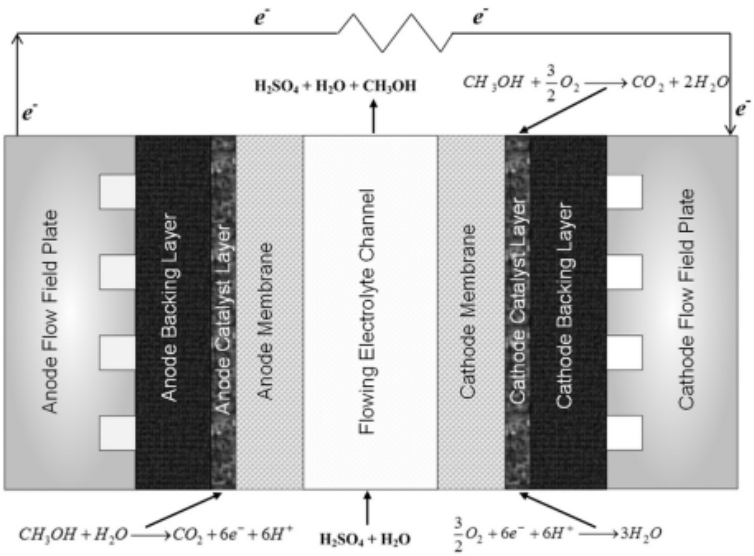

Figure 2.5: Flowing Electrolyte-Direct Methanol Fuel Cell (FE-DMFC) [21]

In the comparison between a Flowing Electrolyte-Direct Methanol Fuel Cell (FE-DMFC) and a conventional Direct Methanol Fuel Cell (DMFC), it is

noted that the power density of the FE-DMFC is slightly lower than that of the DMFC. However, the use of Flowing Electrode Channel (FEC) in the FE-DMFC can significantly decrease the methanol crossover rate. This reduction in methanol crossover has substantial potential to address the issue associated with methanol crossover in these fuel cells.

- **Alkaline Electrolyte Membrane**

  AEM is a type of ion-exchange membrane that only permits the anions to cross the membrane layer [22]. The electrolyte is typically potassium hydroxide (KOH) or similar.

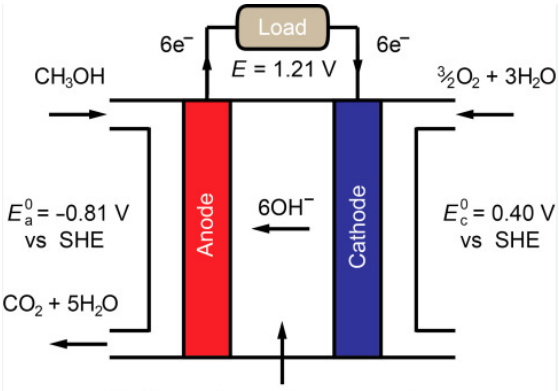

Figure 2.6: Alkaline Direct Methanol Fuel Cell (DMAFC) [22]

As possible to see from the image 2.6, this membrane also drives to different semi-reactions and both the ORR and methanol oxidation are kinetically faster than the DMFC, reducing or avoiding the usage of precious metal catalysts, like Platinum, decreasing the price of the fuel cell:

The anode reaction is:

$$\mathrm{CH_3OH} + 6\,\mathrm{OH^-} \longrightarrow \mathrm{CO_2} + 5\,\mathrm{H_2O} + 6\,\mathrm{e^-} \quad (E_{anode} = 0.40V) \tag{2.4}$$

The cathode reaction is a reduction reaction:

$$\frac{1}{2}\,\mathrm{O_2} + 3\,\mathrm{H_2O} + 6\,\mathrm{e^-} \longrightarrow 6\,\mathrm{H^+} \quad (E_{cathode} = -0.81V) \tag{2.5}$$

The use of an alkaline membrane not only improves the kinetics of these reactions but also addresses corrosion issues under alkaline conditions and enhances volumetric energy density compared to polymer membranes. While the DMAFC with an alkaline membrane shows reduced methanol crossover, it may exhibit slightly lower overall performance compared to traditional PEM-DMFC. [23]

2.1.1.2 Catalyst

In order to provide a solution to the problem of activation overvoltage, cited in the chapter 2.1, a better catalyst should be employed: the most used catalyst was platinum (Pt) in both anode and cathode, which has excellent electrocatalytic performance. However, it faces several negative characteristics, such as high cost, and limited availability and, moreover, it reduces the speed of electrochemical reactions due to the absorption of the intermediates, causing CO poisoning that deteriorates the electrocatalytic activity in the anode side. To mitigate these issues and boost catalytic performance, it's essential to reduce the amount of Pt used. Alloys of metallic are employed to constitute the new catalyst. Different metals have been considered to be mixed with platinum, such as PtOs, PtSn, PtW, and PtMo. Still, the most performance one is ruthenium (Tu), with a Pt:Ru atomic ratio of 1:1, due to its ability to nucleate oxygen-containing species at lower potentials compared to other metals and the ligand effect between Pt and Ru, leading to a more effective and efficient catalytic process for CO electro-oxidation. [24, 25, 26, 27].
Another phenomenon that contributes to the decrease of the voltage approximately by 100 mV at high current, is the diffusion overvoltage. It is related to mass transportation and how liquid fuel can diffuse inside the electrode. The diffusion model could be analyzed through Fick's law [28]:

$$\frac{n_i}{S} = D_i^{eff} \cdot \frac{\partial c_i}{\partial x} \tag{2.6}$$

Where n_i is the molar flow, S is the surface, D_i^{eff} is the effective diffusivity of the molecule i (in this case, the diffusion of methanol in water), c_i is the concentration of the species i, and x is the diffusion distance.

The term D_i^{eff} is directly proportional to the porosity. Therefore by incresing the electrode's porosity, the effective diffusivity (D_i^{eff}) increases, leading to a reduction in the diffusion overvoltage. In simpler terms, higher porosity facilitates more efficient diffusion of the fuel within the electrode. This effect pertains to the decrease in diffusion overvoltage, and by enhancing porosity, the diffusion process is maximised, resulting in improved cell performance at high currents. The most effective way to achieve this is by integrating a porous diffusion layer (DL) as a support structure of the Pt-Ru catalyst. Knowing the thickness of the DL and the concentration on both sides, the equation 2.6 becomes:

$$\frac{n_i}{S} = D_i^{eff} \cdot \frac{c_i - c_i^0}{t} \tag{2.7}$$

The best support structure found is made of carbon material due to their impressive conductivity, extensive surface areas, and stability, such as mesoporous carbon,

carbon black, carbon quantum dots, carbon nanotubes, carbon nanofibre, and graphene. The carbon structure significantly impacts the particle size, shape, and distribution, influencing the dispersion and the metal's adherence to the support. At the moment the carbon most utilized is carbon black, due to its abundance, good distribution of mesopores, and low cost [29].
Non-carbon supported materials are studied, such as Silicon carbide (SiC), Titanium dioxide (TiO), Iridium oxide (IrO_2), Tungsten oxide (WO_3), Tin Oxide (SnO_2). These materials may offer different properties such as superior thermal and chemical stability, corrosion resistance, and dielectric or semiconductive characteristics. However, they are less conductive compared to carbon-based supports and, moreover, more expensive due to complexities in synthesis and processing.

Another technology under research is the heteroatom-doped carbon supports: the activity of carbon catalyst supports can be further enhanced by doping with heteroatoms like nitrogen, sulfur, and boron. This intensive area of study aims to improve the performance of fuel cells [30].

Nowadays, Pt-Ru and carbon black are the current state-of-the-art catalysts and catalyst-support materials in the anode side of fuel cells due to their high electrocatalytic activities during fuel cell reactions.

The fuel cell under-studied in this thesis uses this type of catalyst.

For what concerns the cathode side, here happens the reduction reaction, as shown in equation 2.5. In the literature is possible to see that the most commonly used material is Pt/C for the cathode side [15]. However, for practical and economic reasons, in this case study the cathode catalyst is made of Pt.

2.1.1.3 Gas Diffusion Layer

The Gas Diffusion Layer GDL [28, 31, 32], is a critical component of the DMFC, playing a crucial role in the performance of the fuel cell. It is a thin, roughly 100-400 μm, porous layer, generally made of carbon paper situated between the catalyst layer and the bipolar plate. It is possible to find the catalyst layer directly sprayed in the carbon paper. The main function of the GDLs is to provide a necessary electrical conductivity between the catalyst and the flow channels while facilitating gas diffusion through the catalyst. They have to prevent cell flooding, removing the water produced during the electrochemical reactions, which can hinder gas diffusion to the catalyst, while maintaining some water on the surface to ensure conductivity through the membrane. It is done by treating the face of the carbon paper with hydrophobic materials like Teflon (PTFE). Still, they are able to facilitate heat transfer during cell operation and to provide mechanical strength to hold the MEA together.

2.1.2 Bipolar Plates

The bipolar plates (BPs), shown in Figure 2.7, are thin, conductive plates that electrically separate adjacent cells in a fuel cell stack. Located between the electrodes of the fuel cell, each BP has a conductive surface on either side that allows electricity to flow through the fuel cell.

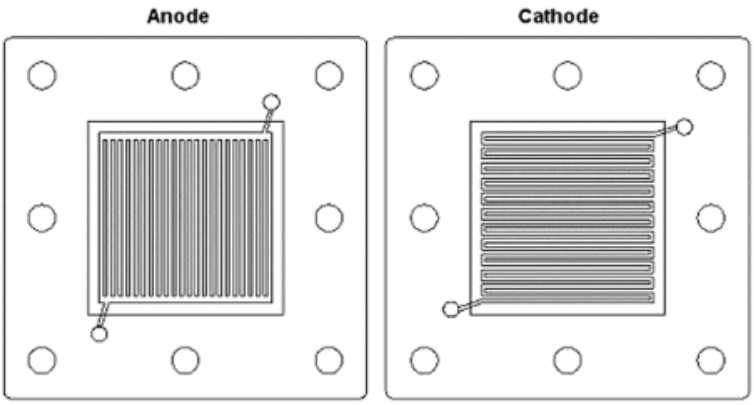

Figure 2.7: Bipolar Plate [33]

These plates are very important as they perform several critical functions, such as maintaining electrical conductivity throughout the stack, ensuring uniform distribution of fuel and oxidant across the electrodes to facilitate efficient reactions, removing effluents (water and other by-products) generated by the chemical reaction within the cell, providing channels for gas flow to facilitate reactant flow and minimise fuel losses and oxidant mixing.

These functions highlight the critical role that BPs play in ensuring the proper operation and efficiency of fuel cells.

BPs are fundamental components in fuel cells, representing 14%-27% of the cost, 60%-80% of the total weight and practically the entire volume of a fuel cell [34].

Materials

Materials for BPs must possess specific characteristics such as high electrical and thermal conductivities, impermeability to reactants and products, suitable mechanical behaviour, low cost, easy machinability and adequate corrosion resistance that is essential for ensuring a long service life of BPs and, more in general, of the fuel cell itself. Carbon-based and metallic materials are studied [34, 35]

- **Carbon-based Materials**:

  The traditional choice for bipolar plates in fuel cells has been graphite due to

its chemical resistance, thermal stability and established use in phosphoric acid fuel cells. However, pure graphite plates suffer from drawbacks such as brittleness, porosity and insufficient mechanical strength, making mass production a challenge. To address these issues, researchers have been investigating graphite-polymer composites, which offer improved corrosion resistance, lower weight and lower cost compared to metallic materials. Various thermoplastic binders such as polypropylene (PP), polyphenylene sulphide (PPS) and polyvinylidene fluoride (PVDF) have been used in graphite-polymer composites for BPs. PP-based composites offer good mechanical properties and low-cost manufacturing but can suffer from poor graphite dispersion due to the lack of polar functional groups in PP, resulting in lower electrical conductivity. PPS has excellent chemical and thermal resistance and recyclability, making it a promising candidate for BP applications. PVDF blends have good bulk conductivity but often lack sufficient flexural strength. Among thermoset binders, phenolic resins have been extensively used for BPs due to their corrosion resistance and ability to operate at elevated temperatures. Graphite materials continue to be investigated for low-cost BPs, with recent studies showing promising results in terms of performance and durability. For example, novel graphite composites and expanded graphite sheets have demonstrated acceptable electrical and mechanical properties, making them suitable for proton exchange membrane fuel cells (PEMFCs). Researchers have also investigated manufacturing processes such as bulk moulding and vacuum resin impregnation to produce graphite-polymer composite BPs with desirable properties.

- **Metallic Material**:

  Metallic materials, particularly stainless steel, offer a promising alternative to graphite for the manufacture of bipolar plates in DMFCs. They are favoured for their lower cost, high mechanical strength, electrical conductivity, ease of fabrication and better resistance to shock and vibration. However, metals are susceptible to corrosion in the harsh operating environment of fuel cells, resulting in excessive interfacial contact resistance (ICR) and high ohmic overpotential. To overcome this challenge, researchers have extensively investigated coatings on metallic BPs. Coatings play a crucial role in mitigating corrosion and improving conductivity. Plates made of stainless steel, titanium, aluminium and several alloys have been tested with different coatings. Electrically conductive amorphous carbon (a-C) coatings applied at high temperatures have been shown to increase electrical conductivity, reduce ICR and improve fuel cell efficiency. Similarly, tin-coated stainless steel BPs have shown improved performance compared to uncoated ones, highlighting the

effectiveness of coatings in mitigating corrosion and improving conductivity. Carbon-based coatings, including pure carbon, carbon-chromium (C-Cr), carbon-chromium-nitrogen (C-Cr-N) and titanium nitride (TiN), have also been investigated for their corrosion resistance and interfacial conductivity when applied to metallic BPs. These coatings have shown promising results in improving corrosion resistance and reducing ICR, thereby improving the performance and durability of metallic BPs. Research has also focused on optimising the design and durability of metallic BPs. Investigations into the ability of stainless steel plates to form low-volume stacks and their long-term durability have shown promising results, indicating the potential for extended service life. Nevertheless, the fact that metals are not as brittle and porous as carbon means that thinner plates can be made.

Flow Field Design

As said before, the main role of the BPs is to supply reactants to the catalyst layers and to remove the reaction products created within the cell. In order to satisfy these requests, each plate is constituting of flow field on both sides, that's why it's called Bipolar plate. In the literature is possible to find different configurations of flow field design [36].

Firstly, an initial classification can be made to differentiate the arrangement of the fluid inlet and outlet connections [37]:

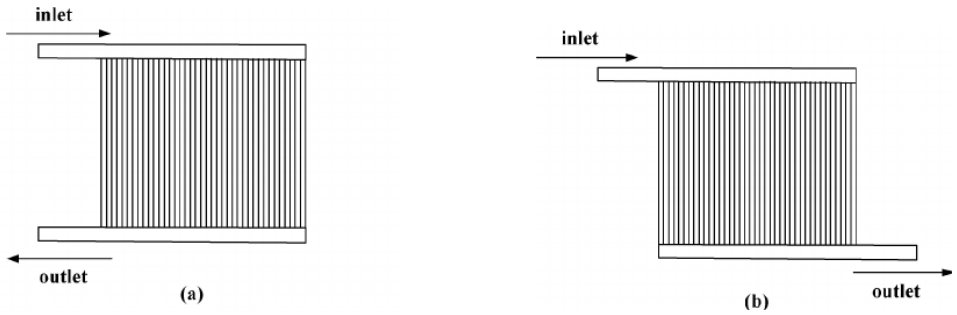

Figure 2.8: Fluid Flow [38]

- U-shape (a): the entry and exit of fluids are concentrated on only one side of the plate, on the head of the DMFC, creating a reverse flow as the outlet gas flows in the opposite direction to the inlet flow.

- Z-shape (b): enter and exit of fluids are situated in opposite headers of the plate; the flow is parallel since both inlet and outlet gases flow in the same direction.

Then the geometry of the flow field can be analysed to understand which is the best configuration to distribute the reactants over the surface of the active area with a uniform concentration, decreasing the pressure drop between the inlet and the outlet of the channels and minimising the parasitic power losses [36]:

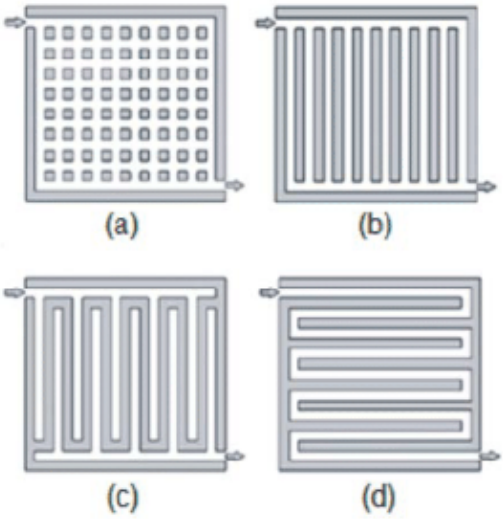

Figure 2.9: Flow field's Geometry: a) Pin-type b) Parallel channels c) Interdigitated d) Serpentine [39]

- Pin-type: pin-type designs are a representative geometry of a flow field without a guided flow path. The pins can be arranged in a line or staggered, and they can be cubic or circular in shape, the former being the most typical. This design ensures a low-pressure drop and mitigates the problem of water droplets blocking individual channels. However, operating the system at high power for long periods of time can result in excessive water production, which can eventually cause the system to flood.

- Parallel channel: in a parallel design, there are multiple parallel paths for the reactant gases from the inlet to the outlet, which reduces the pressure required to push the gases through the system. However, the low pressure of these systems can cause water droplets to accumulate in the flow channels. Over time, these droplets grow and eventually block the channel, causing an uneven distribution of the reactant gases. This in turn creates hot spots that reduce system life and cold spots that reduce overall performance and efficiency. Despite their simplicity and lower pressure drop compared to serpentine designs, parallel designs generally exhibit the lowest overall performance due to these flow distribution issues.

- Interdigitated channels: interdigitated designs do not have a continuous gas flow path from the inlet to the outlet. Instead, they force the gas to flow through the diffusion media, which facilitates the delivery of reactants to the reaction sites and the removal of water. This design appears to manage water more effectively than parallel designs without the excessive pressure drops associated with serpentine designs.
- Serpentine channels: serpentine designs are characterised by a single (or multiple) long, winding path from inlet to outlet. The single-channel design effectively reduces the occurrence of flooding in the channels, as liquid water is continuously expelled by the gas flow. However, the main disadvantage of this design is the increased friction caused by a single long, narrow channel, which requires a higher pressure to drive the gas from the inlet to the outlet. This problem has been overcome by using smaller cells or incorporating additional channels, resulting in parallel serpentine hybrids.

2.1.2.1 End Plate

Positioned at the end of a fuel cell stack, end plates provide structural support, electrical contact for the stack and sealing to prevent gas leakage. End plates are thicker and more robust than bipolar plates because they must withstand pressure and provide reliable electrical contact throughout the fuel cell. The materials used in their construction must provide mechanical strength and electrical conductivity, which can be the same as those used in bipolar plates. End plates may also contain channels for coolant flow to maintain a uniform temperature within the fuel cell stack. They are critical to the structural stability of the fuel cell stack and to the efficient flow of fuel, oxidant and coolant through the cell. However, while bipolar plates primarily distribute fuel and oxidants within the fuel cell, end plates provide structural support, electrical contact and fluid flow management at the end of the fuel cell stack. Both are critical to the efficient and reliable operation of a fuel cell.

Single fuel cells are constructed with end plates only, without the presence of bipolar plates in the centre of the unit. The structure of a single fuel cell is illustrated in the figure 2.3.

The DMFC of this case study consists of plates of 316L steel plates with single-serpentine channels with an active area of 16 cm2.

2.1.3 Applications

DMFCs are emerging as a promising solution for reducing greenhouse gas emissions and combating environmental pollution. These fuel cells offer a clean and sustainable alternative to fossil fuels, as they use methanol as fuel and produce as the only emissions water, which can be reused or recycled within the same fuel cell, and CO_2

which can be stored and used for producing new methanol or for other purposes. DMFCs find wide applications in the world of technology:

- Portable applications: DMFCs are currently the focus of fuel cell research for portable applications such as smartphones, laptops and emergency equipment, as they have characteristics suitable for portable devices. They operate at low working temperatures, have a high energy density, do not require electricity for recharging, use a rapid refuelling system, and have a longer lifespan compared to batteries. DMFCs represent an excellent alternative to the batteries currently in use, especially in scenarios where access to the electric grid for recharging is not available in remote areas [40]. Companies such as Smart Fuel Cell (SFC) and LG Chem are actively researching and commercialising portable devices based on DMFC technology. Methanol-based fuel cells also find application in the field of drones, with companies such as MeOH Power.

- Stationary applications: the stationary application sector also benefits from the use of DMFCs. Company such as "DMFC Corporation", for instance, is involved in developing stationary systems for backup, supplementary, and primary power in situations such as breakdowns, areas with unstable power supply due to grid overload or general instability, and areas with no grid connection.

- Transport applications: DMFCs also have great potential in the transportation sector. German company Ronald Gumper has already designed the first methanol-powered car using this technology. Research is progressing to decarbonise this sector, including maritime and aviation applications.

- Space and military exploration: DMFCs are also suitable for powering military equipment such as radios, night vision devices, and sensors. They are lightweight, compact, and quiet, making them ideal for stealth operations. For example, the US Army has developed a DMFC system for powering soldiers' equipment.

However, although promising, DMFCs still have significant shortcomings that need to be addressed before they can be commercialised on a large scale. These include the aforementioned methanol crossover, which significantly reduces cell performance, the high cost of materials used for platinum catalysts, and the overall weight of the cell, mainly due to the contribution of bipolar plates. Another challenge to overcome is the production of bio-methanol or green methanol, which is currently costly.

2.1.4 Case study's DMFC

The single cell of the DMFC in this case study consists of bipolar plates made of 316L stainless steel, known for its high mechanical strength, electrical conductivity, and ease of mass production through stamping, contrasting with graphite which typically requires more complex mechanical machining processes. These plates feature single-serpentine channels and cover an active area of 16 cm^2. The membrane electrode assembly (MEA) comprises a Nafion® 117 membrane with commercial electrodes supported by Hydrogen Energy carbon paper. The cathode catalyst has a Pt loading of 1 mg/cm^2, while the anode utilizes a Pt-Ru catalyst with a loading of 3 mg/cm^2.

2.2 Air treatment systems

As mentioned above, to produce an electric current, the methanol is injected into the anode side and the air is injected into the cathode side. The methanol molecules dissociate into hydrogen ions which react with the oxygen present in the air. This reaction produces a volume of water which keeps the cathode and anode sides hydrated by migrating towards them. However, as the operating temperature of the fuel cell rises to 60°C, there may be insufficient water in the cell, causing the membrane to dehydrate and requiring a humidification system to increase the performance and life of the unit. On the other hand, excessive humidity in the incoming air can cause flooding of the membrane surface, so effective control of the humidification system is essential to control the water balance within the fuel cell [41, 42].

The air circuit is made of these components:

Compressor

The common air treatment systems used in fuel cells include air compressors or blowers and humidifiers. These components are essential for ensuring the quality of air supplied to the fuel cell. Air compressors or blowers are used to push air into the fuel cell stack. The typical compressors used in these applications are [43]:

- Reciprocating air compressor: increase pressure by compressing the air in one or more compartments before injection.
- Centrifugal compressor: increasing pressure by spinning the air using an impeller or other rotating device.
- Rotary screw compressor: two injecting rotors compressing the medium before injection from the device.

The key decision-making factors in the design and selection of a fuel cell air compressor are the volumetric or mass flow rate, pressure differential (Δp) and electric power consumption.

Sensors and valves

In order to control the performance of the fuel cell, it is fundamental to measure and control values of humidity, pressure, temperature and flow rate of air and water vapour.

Various types of sensors are employed in fuel cells for this purpose [44]:

- Pressure sensors: these sensors monitor the pressure of air entering the fuel cell system, ensuring that it remains within the optimal range for efficient operation. Maintaining proper pressure helps to control the delivery of reactants and the removal of products.
- Temperature sensors: thermocouples, resistance temperature detectors (RTDs), and thermistors are commonly used to monitor the temperature of the air and vapour entering the fuel cell. Accurate temperature control is crucial as it impacts the reaction kinetics and overall efficiency of the fuel cell.
- Humidity sensors: these sensors measure the relative humidity of the incoming air. Proper humidity levels are essential to maintain membrane hydration and avoid drying out or flooding the membrane.
- Flow sensors: to ensure the correct flow rates of air and vapour, flow sensors such as mass flow meters and volumetric flow meters could be used. These sensors help in maintaining the stoichiometric balance of the reactants, optimizing the fuel cell's performance and efficiency.

Valves are also critical components in the air treatment system, playing a role in regulating the flow of gases and maintaining the desired operating conditions.

Maintaining control over these parameters is crucial as it influences the performance, efficiency, and longevity of the fuel cell. Proper valve control ensures the fuel cell operates within its optimal conditions, preventing issues such as membrane drying or flooding.

Heating system

The heating system is a critical component in the air and vapour circuit, especially in environments where the ambient temperature can fall below the optimal operating range of the fuel cell. Heat exchangers, cooling plates, and thermal management systems are widely utilised to keep operating temperatures at optimal levels. Proper

heating ensures that the air and vapour entering the fuel cell reach and maintain the desired temperature, enhancing performance and efficiency.

Maintaining an optimal temperature is essential for several reasons:

- Reaction kinetics: higher temperatures generally increase the reaction rates within the fuel cell, improving efficiency and power output.
- Membrane hydration: proper temperature control helps maintain the hydration level of the membrane, preventing it from drying out or becoming flooded.
- Preventing freezing: in cold climates, a heating system prevents the water in the fuel cell from freezing, which could damage the cell and impede operation.

Humidification

As said before, proper water management is critical in fuel cells to avoid cell flooding and drying within the stack. The inlet air humidity provides the most leverage for controlling the membrane hydration level. If the relative humidity (RH) is too low, the membrane can easily dry out, decreasing proton conductivity and increasing the risk of local hot spots that reduce membrane lifetime. Conversely, excessively humid inlet air can cause flooding of the membrane surface.

External humidification techniques [45]:

- Liquid water transport through membranes.
- Bubblers, which have low control precision and may introduce liquid water to the electrodes.
- Nozzle sprays, which are slow to respond to changes in stack humidity.
- Enthalpy wheels
- Direct injection of liquid or vapour water, enabling control over the amount of water added at the cathode inlet. This is more effective than passive techniques that depend entirely on the fuel cell operating conditions.

Internal humidification techniques [45]: internal humidification relies on self-humidification of the fuel cell, where the reactant streams are humidified directly inside the cell by the water produced in the electrochemical reaction. Performance can be improved by modifying the materials of the MEA or flow channels. However, internal humidification alone results in 20-40% lower performance compared to external humidification with fully saturated inlet gases and is limited to a maximum cell temperature of 70 °C.

Cathode Exhaust Gas Recirculation (CEGR) [46]: CEGR is a promising active humidification approach that uses the water vapour in the cathode exhaust

to humidify the inlet air. By varying the amount of recirculated exhaust, the RH at the stack inlet can be modulated. Experimental results have shown that CEGR significantly improves PEMFC system performance, efficiency and durability compared to passive humidification.

Summarizing, while internal self-humidification can provide accurate control in variable conditions, it is limited to low temperatures. External humidifiers enable better performance at high temperatures but add complexity and parasitic losses to the system. CEGR offers an attractive balance of performance and control as an active humidification method.

2.2.0.1 Commercial solution

To further explore the practical application of air treatment systems in fuel cells, it is essential to examine specific commercial solutions such as those offered by Cellkraft. These systems are meticulously designed to address critical challenges in fuel cell operation, including precise control of humidity levels, efficient air supply, and temperature management.

Cellkraft's solutions are tailored to significantly enhance the performance and longevity of fuel cells through advanced humidification and air management technologies. Through extensive case studies and field applications, Cellkraft has demonstrated the efficacy of their solutions across various fuel cell technologies, from proton exchange membrane fuel cells (PEMFCs) to direct methanol fuel cells (DMFCs). Their systems play a pivotal role in enhancing system reliability, efficiency, and environmental sustainability in both stationary and mobile fuel cell applications.

Cellkraft P-Series Air Treatment System

The Cellkraft P-Series, shown in figure 2.10, represents an advanced air treatment solution specifically designed to optimise fuel cell performance. This system integrates advanced technologies to ensure precise control over humidity levels and air temperature, essential for enhancing operational efficiency and longevity in various applications.

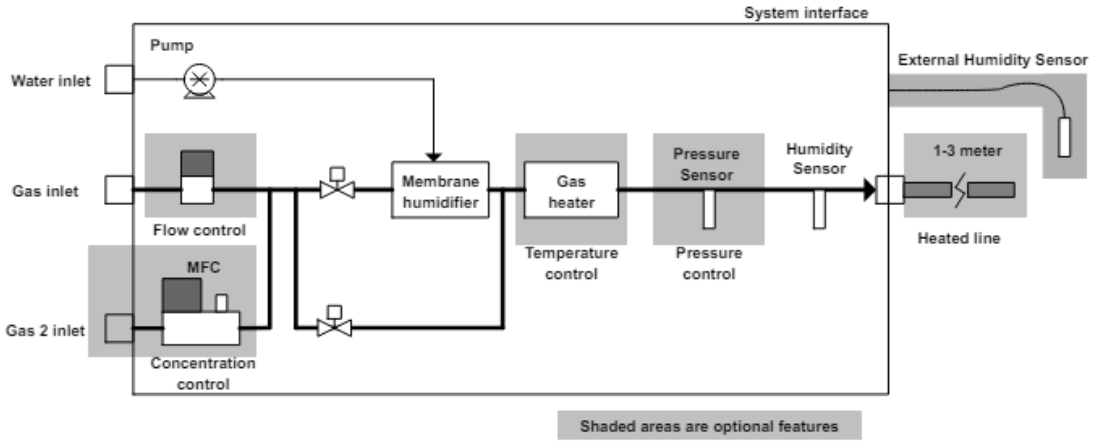

Figure 2.10: P-Series of Cellkfraft

As it possible to see in Figure 2.10, the P-Series employs a membrane humidifier to introduce moisture into the air stream, complemented by a heater that finely regulates air temperature. These parameters are continuously monitored and adjusted via feedback control loops to maintain optimal conditions for fuel cell operation. Designed to handle flow rates ranging from 0 to 250 litres per minute and pressures up to 20 bar(a), the P-Series enables independent control of air humidity and temperature, allowing precise optimisation of fuel cell performance under varying operational conditions.

In demanding environments such as fuel cell test facilities, industrial production laboratories and environmental simulation chambers, the P-Series excels at fine-tuning air parameters to ensure peak performance and durability of fuel cell systems. Its robust design and automated control features help to reduce maintenance costs and extend component life.

At the heart of the P-Series is Cellkraft's advanced membrane humidification technology, renowned for its consistent performance over a wide range of flow rates. This technology uses a water-permeable membrane to efficiently transfer moisture from a reservoir to the air stream, ensuring consistent operation without the risk of droplet formation. By integrating these solutions, Cellkraft enables users to achieve superior performance and reliability in both stationary and mobile fuel cell applications, while promoting environmental sustainability through precise air management capabilities.

The Cellkraft P-Series is a testament to innovation in air handling systems, offering unparalleled control of humidity and temperature to optimise fuel cell operation. With its robust design, advanced technologies and application-specific adaptations, the P-Series continues to redefine the standards in fuel cell technology.

However, while the Cellkraft P-Series represents a promising solution for optimising fuel cell performance, it may not be suitable for large-scale fuel cell applications due to its limited capacity. To address this limitation, this thesis work focuses on developing an innovative air treatment system that can be scaled up to meet the demands of large-scale fuel cell systems, such as those used in transportation or grid-scale energy storage. By designing a more scalable air treatment solution, this research aims to further advance the integration of fuel cells with renewable energy sources and support the transition to a sustainable energy future.

Chapter 3

Design requirements

The main objective of the study is to design an air treatment system that provides controlled air to the cathode of DMFCs with precise regulation of temperature, humidity, and mass flow rates. These parameters are critical for understanding and optimizing fuel cell performance.

3.1 Operational requirenment

The operational requirements outlined here are based on the specifications provided by the client, who requires the implementation of an air treatment system for the fuel cell test bench. The primary objective is to design a system that precisely controls temperature, humidity and mass flow rates to deliver controlled air to the cathode of DMFCs. These parameters are critical to understanding and optimising fuel cell performance.

3.1.1 Mass Flow Rates:

- Oxygen-to-methanol ratio corrected to $1.5\,\mathrm{kg_{O_2}/kg_{MeOH}}$.
- Single-cell and 3-MEA stack dosing:
  - Air Mass Flow: 0.4-1.9 g/min (Optimal: up to 2.6 g/min). [0.1 and 4.333 10^{-5} kg/s]
  - Air Volumetric Flow: 380-1571 ml/min (Optimal: up to 2200 ml/min).

3.1.2 Temperature and Humidity Range:

- Operating Temperature: 20-80 ºC.
- Humidity Range: 20-100 %.

3.1.3 Calculation

3.1.3.1 Mass Flow Rates

In order to achieve these results some calculations are carried out.

$$\mathrm{CH_3OH} + \frac{3}{2}\,\mathrm{O_2} \longrightarrow \mathrm{CO_2} + 2\,\mathrm{H_2O} \tag{3.1}$$

From the overall equation of the electrochemical reaction 3.1, seeing the stoichiometric of it, the mass relationship between methanol and dry air can be obtained:

$$\frac{m_{air}}{m_{CH3OH}} = \frac{n_{O_2}}{n_{CH3OH}} \cdot \frac{n_{air}}{n_{O_2}} \cdot \frac{M_{air}}{M_{CH3OH}} \tag{3.2}$$

Remembering the composition of dry air:

- 78.09% nitrogen N_2
- 20.95% oxygen O_2
- 0.93% argon Ar
- 0.03% carbon dioxide CO_2 and other gases

Therefore the mole fraction of O_2 in air:

$$x_{O_2} = 0.2095 \tag{3.3}$$

$$\frac{n_{air}}{m_{O_2}} = \frac{1}{0.2095} = 4.76 \tag{3.4}$$

Therefore, for every 1 kmol of O_2 there are approximately 4.76 kmol of air.

- $M_{air} = 28.96\ \mathrm{kg_{air}/kmol_{air}}$
- $M_{CH_3OH} = 32.04\ \mathrm{kg_{CH_3OH}/kmol_{CH_3OH}}$
- From 3.1 the stoichiometric coefficient is $\mathrm{n_{O_2}/n_{CH_3OH}} = 3/2$ since 1 mol of CH3OH requires 1.5 mol of O2

$$\frac{m_{\mathrm{air}}}{m_{\mathrm{CH_3OH}}} = \frac{3}{2} \cdot 4.76 \cdot \frac{28.95}{32.04} = 6.456\,\mathrm{kg_{air}/kg_{CH_3OH}} \tag{3.5}$$

The mass flow rate of the oxidant defined for the system has to be capable of feeding DMFC devices from a single cell to a three-cell stack with a maximum

voltage of 10 V and 8 A of maximum current. Through Faraday's equation the mass consumption rate of methanol can be estimated with:

$$\dot{m}_{\mathrm{CH_3OH}} = \frac{I \cdot N_{cell}}{z_{CH_3OH} \cdot F \cdot \eta_F} \cdot M_{\mathrm{CH_3OH}} = 1.328 \times 10^{-6}\,\mathrm{kg/s} \tag{3.6}$$

Considering the current $8A$, the Faraday's constant F=96485 C/mol, the exchanged mol of electrons for each mol of CH3OH $z_{CH_3OH} = 6$, the fuel efficiency $\eta_F = 1$:

For a single cell operating at 8 A:

$$\dot{m}_{\mathrm{CH_3OH}} = 4.427 \times 10^{-7}\,\mathrm{kg/s} \tag{3.7}$$

The corresponding air mass flow rate:

$$\dot{m}_{air} = 4.427 \times 10^{-7}\,\mathrm{kg/s} \cdot 6.456 = 2.867 \times 10^{-6}\,\mathrm{kg/s} \tag{3.8}$$

For a stack of three cells:

$$\dot{m}_{\mathrm{CH_3OH}} = 1.328 \times 10^{-6}\,\mathrm{kg/s} \tag{3.9}$$

The corresponding air mass flow rate:

$$\dot{m}_{air} = 1.328 \cdot 10^{-6} kg/s \cdot 6.456 = 8.567 \cdot 10^{-6} kg/s \tag{3.10}$$

The lower limit of the air mass flow rate is set at $0{,}1 \cdot 10^{-5}\,\mathrm{kg/s}$ to account for the limitations of component accuracy and to avoid issues related to measurement precision. The upper limit is established at $4.333 \cdot 10^{-5}\mathrm{kg/s}$ to provide a sufficient margin for future experiments involving higher currents or increased cell counts. This approach ensures that the system is prepared to handle a range of operating conditions while maintaining accurate control over the airflow.

3.1.3.2 Temperature and Humidity

Unpressurised DMFCs typically operate at temperatures below 80°C. The reason is that raising the temperature above this value can lead to component degradation, methanol evaporation and an increased likelihood of methanol crossover, where methanol diffuses through the membrane without reacting. With this in mind, the operating temperature range should be kept between 20ºC and 80ºC to avoid the need for an expensive air cooler.

Regarding moisture, the humidity range should reach any value from the humidity of the air available in the room until saturation, to avoid the need for a costly dehumidifier.

Chapter 4

Concept Egineering

The air treatment system will draw air from the laboratory environment. However, the fuel cell requires higher temperature and humidity levels than those available in the laboratory atmosphere. To achieve these conditions, two processes are necessary: heating the air and mixing it with the precise amount of steam to reach the desired temperature and humidity. This creates a dilemma: is it better to humidify first and then heat (4.1), or to heat first and then humidify (4.2)? To determine the optimal configuration, we can test if it is possible to achieve the most extreme conditions of the temperature and humidity intervals specified in the design requirements, in the previous Chapter 3 with either of the two possible configurations. This can be done by applying the given set of equations, presented in Chapter 5.1, to both configurations. If any incompatibilities arise in the results, the corresponding configuration can be discarded. The first configuration mixes the air and steam coming from two different circuits, then heats them and sends them to the fuel cell.

In Chapter 5.1 the thermodynamic values have been studied, revealing that the relative humidity Φ of the mixture was greater than one, particularly 234 % founded by the equation 5.5. This is due to the fact that the initial low temperature of the air prevented the necessary molar fraction of water in the vapour phase from being absorbed. As a result, the air becomes supersaturated and water condensation occurs. In table 5.1 the values of each point of the configuration are given, where 1a is the air at the laboratory conditions, 2ha is the moisture air, 3ha is the heated moisture air, and 1w is the vapour condition.

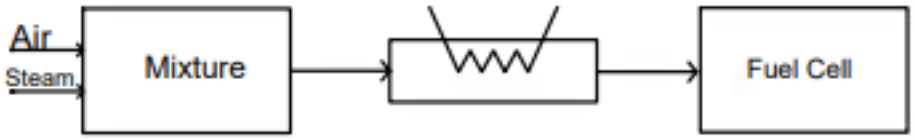

Figure 4.1: Fist Configuration

Table 4.1: Value at ambient condition

fluid	T [°C]	p [kPa]	Φ [%]	$\omega \times 10^3\,\mathrm{kg_v/kg_a}$
1a	25	100	40	7.99
2ha	60	100	234	549.8
3ha	80	100	99	549.8
1w	99	100	/	/

A second and final configuration has been carried out bringing to more appropriate values, founded through the equation of Chapter 5.1: before mixing the two fluids the air is warmed up through the resistance and then humidified. It is verified that the boundary conditions are adequately satisfied, and no condensates are produced at the exit of the humidification stage. In the table 4.2 the values of each point of the configuration are given.

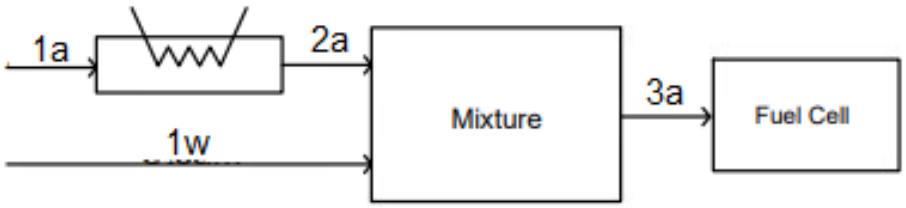

Figure 4.2: Final Configuration

Table 4.2: Value at ambient condition

fluid	T [°C]	p [kPa]	Φ [%]	$\omega \times 10^3\,\mathrm{kg_v/kg_a}$
1a	25	100	40	7.99
2a	63	100	5.5	7.99
3ha	80	100	99	548.9
1w	99	100	/	/

Chapter 5

Model

5.1 Thermodynamic model

As said in Chapter 4, to modify the conditions of an ambient air stream, achieving the desired humidity and temperature during each test, the air treatment process in the designed system involves heating the ambient air in a first stage and subsequently introducing steam into the preheated air stream to achieve the desired humidity and temperature conditions during each test. In Figure 5.1 the diagram of the engineering concept used for the defined air treatment system is shown.

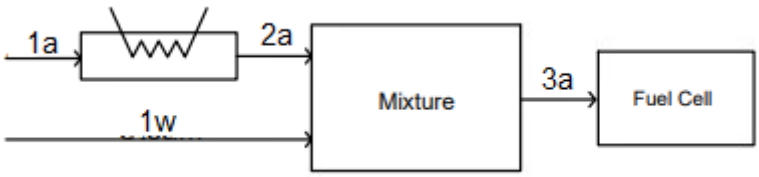

Figure 5.1: Flowrate

To better imagine the fluid flow, the scheme of the circuit is provided in Figure 7.10, described in detail in Chapter 6.

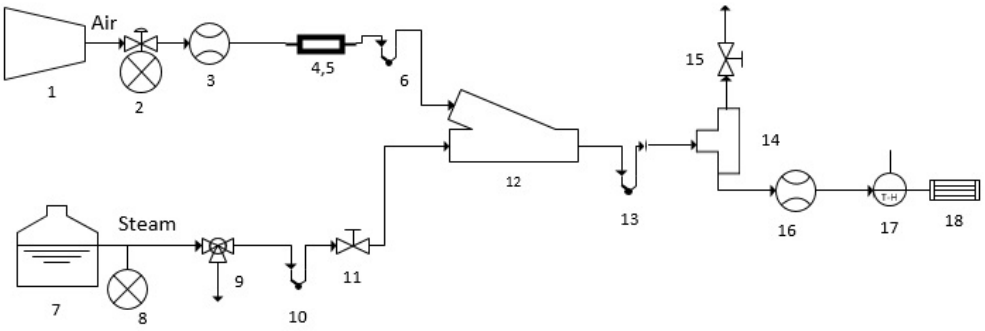

Figure 5.2: Circuit Scheme

In order to understand which are the conditions of air and vapour that the system has to work with, a thermodynamic model has to be studied.

The values of temperature, pressure and the relative humidity (RH) Φ, defined as the ratio between the partial pressure of water vapour (p_v) and the saturation vapour pressure (p_{sat}) at a given temperature, of each point of the above circuit 5.1 are illustrated in the table below 5.1:

Table 5.1: Value at ambient condition

fluid	T [°C]	p [kPa]	Φ [%]
1a	25	100	40
2a	63	100	5.5
3ha	80	100	99
1w	99	100	/

The fluid relative to 1a in Table 5.1, is air extracted from the laboratory environment by an air compressor, heated by electrical resistance, relative to condition 2a, where the value of the temperature is found through the enthalpy calculated with the mass and energy balance, equations 5.1 and 5.2, while the saturated vapour, 1w, comes from a pressure cooker, and then the mixture, 3ha, enters the fuel cell. The values of temperature, pressure and RH of fluid 1a are measured and considered as standard conditions. The temperature of the fluid 3ha is set at 80 °C, as it is a constraint of the fuel cell, that has to work at this temperature. The relative humidity, ρ, is calculated through the formula 5.5.

In order to calculate the temperature at point 2a, the mass and energy balance should be applied:

Mass Balance applied to the mixing chamber of the figure 5.1:

$$\dot{m}_w = \dot{m}_a(\omega_{3ha} - \omega_{2a}) \tag{5.1}$$

Energy Balance, First Law of Thermodynamics applied to the mixing chamber of the figure 5.1:

$$\dot{Q} + \dot{W} = \left.\frac{\partial E}{\partial t}\right|_{cv} + \sum \dot{m}_{out} \cdot h_{out} + \sum \dot{m}_{in} \cdot h_{in} \tag{5.2}$$

Considering the assumptions of an adiabatic mixing chamber and steady-state flow, it is obtained:

$$\begin{aligned} 0 &= \sum \dot{m}_{out} \cdot h_{out} + \sum \dot{m}_{in} \cdot h_{in} \\ &= \dot{m}_a[h_{3ha} - h_{2a} - h_w(\omega_{3ha} - \omega_{2a})] \end{aligned} \tag{5.3}$$

from which it is obtained:

$$h_{2a} = h_{3ha} - h_w(\omega_{3ha} - \omega_{2a}) \tag{5.4}$$

In order to understand the process of the circuit, the thermodynamic values of these fluids are studied:

- Saturation pressure p_{sat}: refers to the pressure at which a phase change occurs at a given temperature, found in thermodynamic tables [47].
- Partial pressure p_v, p_a: is the pressure that n_i moles of component i would exert if the component were alone in volume V at the mixture temperature T.

$$\Phi = \frac{p_v}{p_{sat}} \qquad\qquad p_v = p_{sat} \cdot \Phi \tag{5.5}$$

$$p_a = p_{tot} - p_v \tag{5.6}$$

- Humidity ratio ω: defined as the ratio of the mass of the water vapour to the mass of dry air.

$$\omega = \frac{m_v}{m_a} = \frac{M_v}{M_a} \cdot \frac{p_v}{p_a} = \tilde{\omega} \cdot \frac{p_v}{p_a} = 0.622 \cdot \frac{p_v}{p_a} \tag{5.7}$$

- The density of air is easy found in the thermodynamic table [48], while the density of the overall mixture behaves according to the ideal gas equation of state:

$$pV = nRT \tag{5.8}$$

  Where p is the pressure, V is the volume, n is the number of moles, R is the gas constant and T is the temperature.

Each component of the mixture acts independently. The total pressure of the mixture is the sum of the partial pressures of the dry air and the water vapour:

$$p = p_a + p_v \tag{5.9}$$

Where p_a is the partial pressure of dry air, and p_v is the partial pressure of water vapour, values found on table 5.2.

Applying the ideal gas law to the components separately:

$$\begin{aligned} p_a V &= n_a R T \\ p_v V &= N_v R T \end{aligned} \tag{5.10}$$

The partial pressures can be expressed in terms of mole fractions:

$$\begin{aligned} p_a &= y_a p \\ p_v &= y_v p \end{aligned} \tag{5.11}$$

where y_a and y_v are the mole fractions of dry air and water vapour, respectively.

The molecular weight of the mixture M_{mix}:

$$M_{mix} = \frac{\sum m_i}{\sum n_i} = \frac{m_a + m_v}{n_a + n_v} = \frac{\frac{m_a + m_v}{m_a} \cdot M_a}{\frac{n_a + n_v}{n_a} \cdot (1 + \tilde{\omega})} \tag{5.12}$$

Where $\tilde{\omega} = n_v / n_a$

Therefore, the density is:

$$\frac{1}{v} = \rho = \frac{p}{R_{ah} \cdot T} = \frac{p}{\frac{R_V}{M_m} \cdot T} = \frac{p}{\frac{R_v}{\frac{1+\omega}{1+\tilde{\omega}} \cdot m_a} \cdot T} = 0{,}848\,\mathrm{kg/m^3} \tag{5.13}$$

Table 5.2: Value of pressures

fluid	P_{sat} [kPa]	p_v [kPa]	p_a [kPa]	$\omega \times 10^3\,\mathrm{kg_v/kg_a}$	ρ [kg/m^3]
1a	3.17	1.27	98.73	7.99	1.184
2a	23.033	1.27	98.73	7.99	1.059
3ha	47.39	46.91	53.08	550	0.848

- The values of enthalpy of saturated vapour h_v are found in thermodinamics table [47]. The values of the enthalpy of the dry air h_{1a} are found through the Forluma 5.14, considering the air as an ideal gas because it simplifies calculations and is sufficiently accurate for many engineering applications, especially at moderate temperatures and pressures where real gas deviations are minimal.

$$h_a = c_p \cdot T, \quad c_p = 1.005 \left[\frac{kJ}{kg \cdot C}\right] \tag{5.14}$$

$$h = h_a + \omega \cdot h_v \tag{5.15}$$

Table 5.3: Value of Entalpy [47]

fluid	h_a [kJ/kg$_a$]	h_v [kJ/kg$_v$]	h [kJ/kg$_a$]
1a	299.64	2547.2	320
2a	337.97	2618.33	358.34
3ha	354.92	2643.7	1809.53

5.2 Proportional Integral Derivative controller - PID

As mentioned above, it is necessary to heat the air entering the fuel cell, as it operates at 80°C, in order to favour the chemical reaction inside and the generation of electricity. For this purpose, an electrical resistance and a system of sensors to measure the temperature and humidity of the air are used.

Intending to pilot the electrical circuit, a Proportional Integral Derivative controller (PID) is used. It is an algorithm used in industrial applications that uses a control loop feedback mechanism to control process variables. It is the most accurate and stable controller. The aim of this algorithm is to control a process variable, like temperature, pressure, flow rate, speed, etc and set it to a set point, r. The difference between the process variable and the set point is the error e, used by the control system algorithm to determine the desired output to drive the plant.

The PID control is composed of three contribution:

- Proportional: it applies a multiplier known as the gain, K_p, to the value of the direct difference between the measured state and the desired state

$$u(t) = K_p \cdot e(t) \tag{5.16}$$

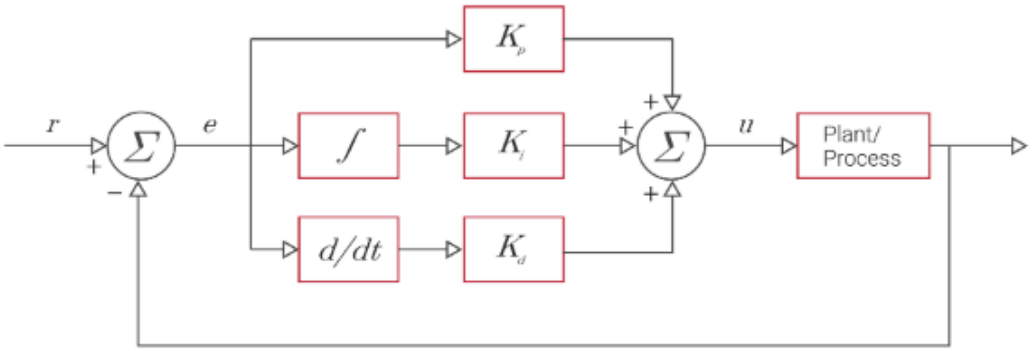

Figure 5.3: Feedback system

- Itegral: it integrates the error between the desired state and the measured state over time and scales this by a gain value, K_i

$$u(t) = K_i \int_0^t e(t)\,dt \tag{5.17}$$

- Derivative: it responds to the rate of change of the error signal

$$u(t) = K_d \frac{de(t)}{dt} \tag{5.18}$$

Each of these contribution are then summed together and used to calculate an input to the system being controlled to drive the dynamics of the system to the desired state.

5.2.1 Electrical circuit

Referring to the practical case of this thesis, the PID control is accomplished using the software Arduino IDE. It controls a resistance which must keep the air temperature fixed at 60°C, while the temperature is read by a sensor MAX6675 throughout a thermocouple. In Figure 5.4 it is possible to see the connections between the sensors and the Arduino Hardware.

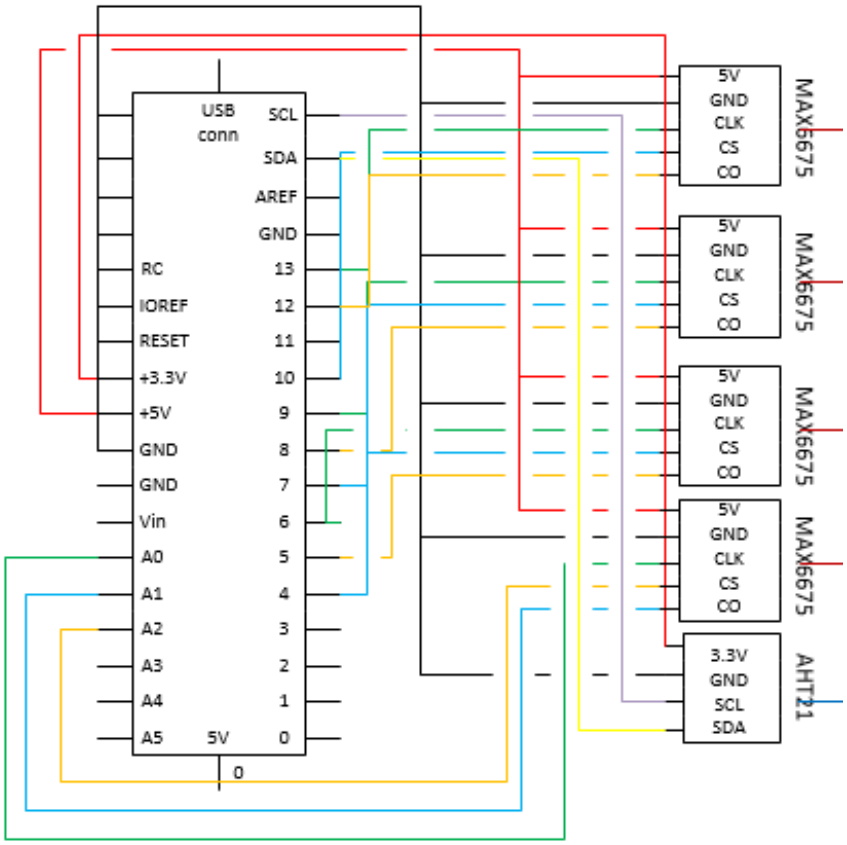

Figure 5.4: Arduino connections

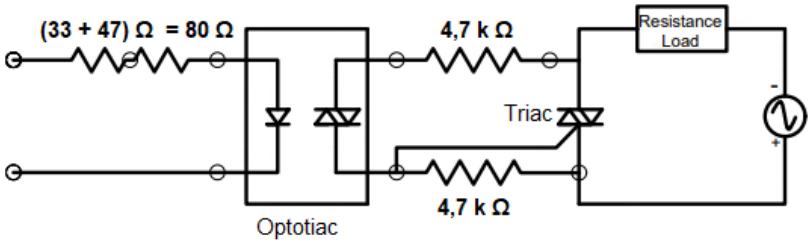

Figure 5.5: Electrical Circuit

In the electrical circuit shown in Figure 5.5 that drives the resistance, it is possible to distinguish 3 components:

Triac

From the acronym Triode for Alternating Current, triac is a semiconductive and electronic component, widely used in AC power control. Is able to switch high voltages in high levels of current over both parts of an AC waveform. When the triac receives a control signal from the PID, it allows current to flow until the signal is removed. This allows very precise control of the power supplied to the resistance, thus regulating the temperature efficiently. Basically, the purpose of this device is to switch the current ON/OFF and turn on the electrical resistance.

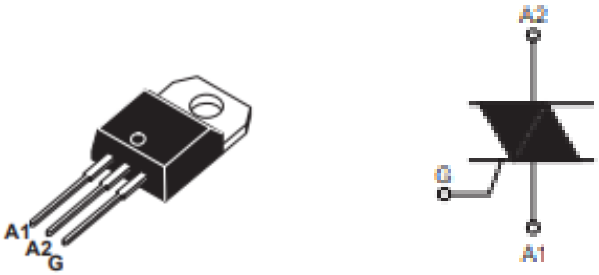

Figure 5.6: Triac

The Triac used in this project is **BTA06** and, as it is possible to see from the above figure, it has three terminals: two anodes (A1, A2), or main terminals, and the gate (G).

Optotriac

An optotriac is a semiconductor device that allows an electrical signal to be transmitted between two isolated circuits. It consists of gallium arsenide infrared emitting diodes on the input side optically coupled to a silicon bilateral switch (photosensitive triac). When the infrared emitting diodes are illuminated, they trigger the photosensitive triac, allowing current to flow in the output circuit (typically an AC circuit). In this project the optotriac used is the **MOC3021**, it is designed to isolate and protect low-voltage or low-power circuits from high-voltage or high-power circuits, so, in this case, it is used to protect the Arduino part, that works with 5V, from the triac, that works with 220V.

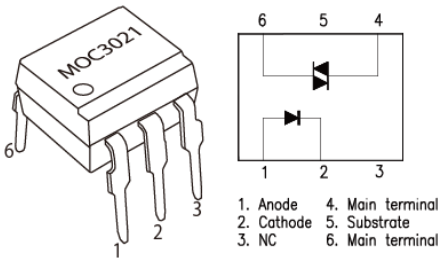

Figure 5.7: Optotriac

Arduino UNO

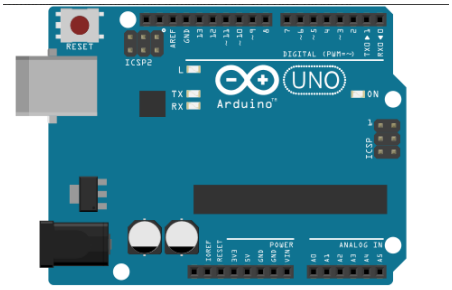

Figure 5.8: Arduino UNO

To control the entire circuit, it is necessary a microcontroller, the brain of the circuit. Arduino UNO is a free hardware electronic board incorporating a reprogrammable microcontroller (**ATmega328P**) and a series of female pins. These allow connections between the microcontroller and the various sensors and actuators to be established very easily. It is piloted through a code (called sketches) written with the software Arduino Integrated Development Environment (IDE). IDE allows the PC to be used to write the programme, compile it and transfer it, via a USB connection, to the Arduino.

A breadboard is necessary to connect all the sensors, triac and optotriac to the Arduino.

Chapter 6

Basic and detailed engineering

Basic engineering involves the initial stages of a project, focusing on defining the overall scope and technical feasibility. It includes the preliminary design and planning, which lays the groundwork for detailed engineering. This phase aims to establish the fundamental concepts and determine the project's viability.

Detailed engineering delves into the specificities of the project, transforming the conceptual plans from basic engineering into detailed and executable designs. This phase involves comprehensive and precise design documents, detailed drawings, and technical specifications necessary for construction, procurement, and installation. The primary objective is to ensure all aspects of the project are fully designed and documented to avoid any ambiguities during implementation.

6.1 Piping and Instrumentation Diagram - P&ID

The P&ID is a critical component of both basic and detailed engineering. It illustrates the layout of the system, showing how each component is interconnected. This visual aid is essential for understanding the overall design and functionality of the air treatment system.

Looking at the figure 6.1, it is possible to follow the paths of the fluids and individuate the components of the circuit: the air compressor (1) takes air from the lab, and then a pneumatic regulator (2) and a flowmeter (3) adjust it. After that, the air is heated by a PID controlled electric resistance (4). A temperature sensor (5) is twisted around the resistor to monitor its temperature, which will drive a PID controller via Arduino IDE. Another temperature sensor (6) monitors the temperature of the gas flow after it passes through the electric resistor and before it goes into the mixing chamber (12). Meanwhile, the second stream, based

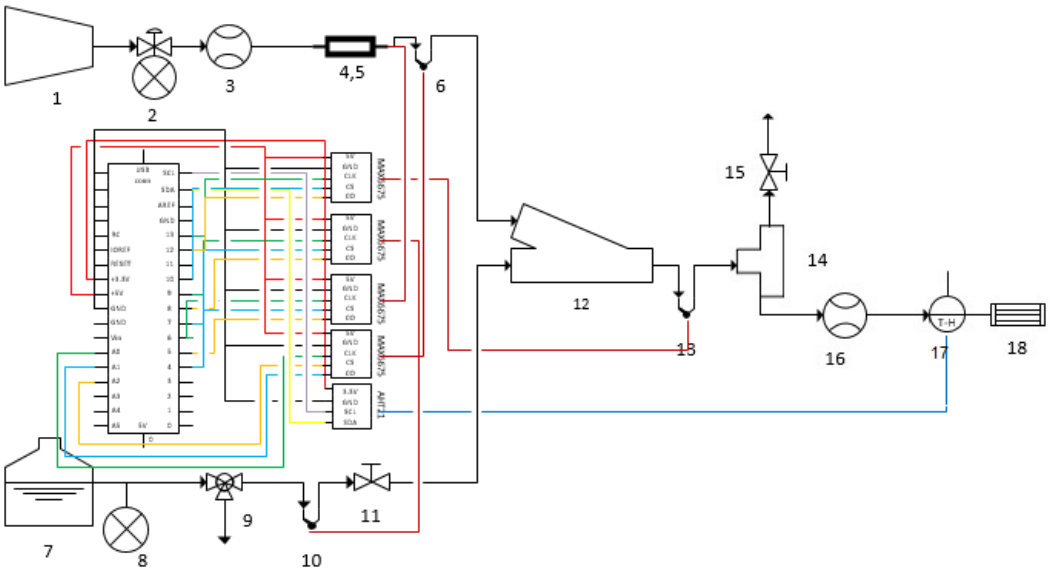

Figure 6.1: P&ID

on saturated steam, is generated on a high-pressure steam generator, composed of a pressure cooker (7). The pressure of this stream is controlled by a pressure gauge (8). After the pressure control by the pressure gauge, a hydraulic ball valve (9) regulates the path of the stream before the control of temperature through a temperature sensor (10), then its path is regulated by a hydraulic flow control valve (11) and its entrance into the mixture chamber (12). Once the air mixture exits from the mixture chamber (12) there is another temperate sensor (13) followed by a T connection (14). This connects the circuit to a hydraulic flow control valve (15) and a mass flowmeter (16). After the flowmeter, the temperature and humidity sensor (17) is placed just before the fuel cell (18) to measure the actual condition of the humid air before it enters.

To prevent water from condensing on the steam line when components are cold, a preheating procedure has been designed. A constant wattage heating cable is used, twisted along the entire length of the tube occupied by the steam section.

6.2 Component specifications

Detailed specifications of the components are crucial. Below is a list of the technical specifications, including the type of sensors and other electric components.

1. **Compressor**: 6 l, 8 bar max, 1.1kW piston compressor oil free to avoid air contamination.

Figure 6.2: Compressor

2. **Pneumatic regulator**: 0.01 MPa → 0.8 MPa. To regulate the pressure of the air. Attached to this there is a pressure gauge to read the actual pressure (0 bar → 1.6 bar max).

Figure 6.3: Pneumatic regulator

Figure 6.4: Pressure gauge

3. **Flowmeter**: To measure the air mass flow rate (0,4 l/min → 5 l/min).

Figure 6.5: Flowmeter

4. **Tubular finned heater for air**: 200 W, 230 V A.C. It is within a case made of stainless steel and 3D printed materials with ABS material.

Figure 6.6: Electric resistance

5. **Pneumatic connection**: necessary to insert a thermocouple to measure air temperature.

Figure 6.7: Pneumatic connection

6. **Pressure cooker**: to generate steam.

Figure 6.8: Pressure cooker

7. **Induction plate**: to warm up the pressure cooker.

Figure 6.9: Induction plate

8. **Hydraulic ball valve**: a three-way valve to purge excess steam.

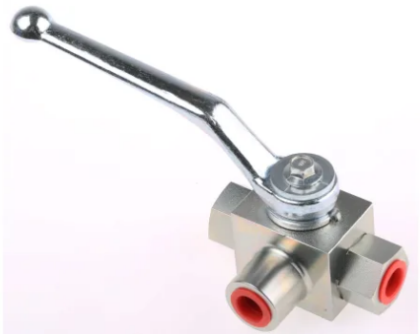

Figure 6.10: Hydraulic ball valve

9. **Hydraulic flow control valve**: 6.11 max. 50 L/min, 350 bar max, Steel.

Figure 6.11: Hydraulic flow control valve

10. **Component for mixture**: air and steam meet in a plastic chamber 3D printed with ABS.

Figure 6.12: mix chamber

11. **Flowmeter**: to measure the steam quantity.

Figure 6.13: Vapour Flowmeter

12. **Copper pipe**: 112 bar max, 10m length, outer diameter 6mm.

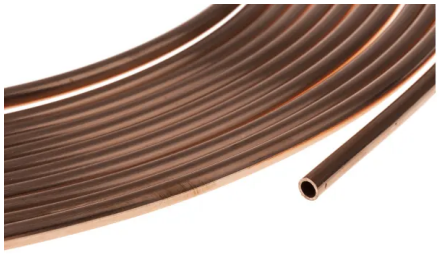

Figure 6.14: Copper pipe

13. **Compressed air hose**: made of Nylon, Ø int. 2.5mm, Ø ext. 4mm, length 30m.

Figure 6.15: Compressed air hose

14. **Arduino UNO**: to control the electrical part Figure 5.8.

15. **Sensor MAX6675**: to measure the temperature of air and steam through a thermocouple.

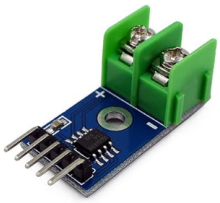

Figure 6.16: Sensor MAX6675

16. **Sensor AHT21**: to measure the temperature and steam of the mixture.

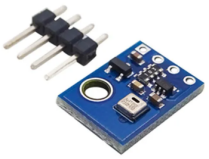

Figure 6.17: Sensor AHT21

17. **Thermocouple type K**: Maximum temperature +400°C.

Figure 6.18: Thermocouple

18. **Constant wattage heating cable**: 6 m, 10 W/m, temp. -70→+200°C. To warm up the steam part.

Figure 6.19: Heating cable

19. **Thermostat AKO-D14123**: To control the temperature of the heating cable.

Figure 6.20: Thermostat

20. **Watertight box IP55**: cover with screws, with cones, 153 x 110 x 70 mm. To contain the thermostat and the cables.

Figure 6.21: Box

21. **Aluminium tape**: for attaching high-temperature materials

Figure 6.22: Aluminium tape

22. **Pipe insulation**: To limit the losses.

Figure 6.23: Pipe insulation

23. **Fitting**: Figure 6.24 is the fitting in the air circuit, since it can handle -20 to 80 °C, Figure 6.25 is the fitting for the vapour circuit, since it can handle -20 to 120 °C, Figure 6.26 is the fitting for inserting the thermocouples in the circuit.

Figure 6.24: Air circuit fitting

Figure 6.25: Vapour circuit fitting

Figure 6.26: Thermocouple Insertion Fitting

6.3 Sizing components

The sizing of system components is a critical aspect of the design process, ensuring that each part operates efficiently under the most demanding conditions. For the system under study, the most challenging operating conditions correspond to a target relative humidity $\Phi = 1$ and a temperature $T = 80°\text{C}$. These conditions necessitate a comprehensive analysis to accurately determine the dimensions of the air and steam flowmeters and other system components.

Under these specified conditions, the maximum dry air mass flow rate is $4{,}333 \cdot 10^{-5}\,\text{kg/s}$, as outlined in paragraph 3.1.3.1. To heat the air from 25°C to 80°C, we need to use the specific heat capacity of air which is $c_p = 1{,}0005\,\text{kJ/kgK}$ The energy required (Q) to heat the air can be calculated using:

$$\begin{aligned} Q &= \dot{m}_a \cdot c_p \cdot \Delta T \\ &= 4.333 \times 10^{-5}\,\text{kg/s} \cdot 1.005\,\text{kJ/kgK} \cdot (353.15 - 298.15)\,\text{K} \\ &= 2.395\,\text{W} \end{aligned} \tag{6.1}$$

This calculation assumes that the air is dry and behaves as an ideal gas. It is important to state these assumptions explicitly. The ideal gas model is used because it simplifies calculations and is sufficiently accurate for many engineering applications, especially at moderate temperatures and pressures where real gas deviations are minimal.

For what concerns the the mass flow rate of steam, the most critical value is $\dot{m}_v = 2{,}387 \cdot 10^{-5} kg/s$, value found from:

$$\omega = \frac{m_v}{m_a} \tag{6.2}$$

$$m_v = \omega \cdot m_a = 0.551 \cdot 4{,}333 \times 10^{-5}\,\text{kg/s} = 2.387 \times 10^{-5}\,\text{kg/s} \tag{6.3}$$

To generate moist air - this term refers to a mixture of dry air and water vapour, where the dry air is treated as if it were a pure component - we need to consider the phase change enthalpy of vaporisation Δh for water, which is about $2260 kJ/kg$. The energy required (Q_v) for vaporisation can be calculated using:

$$\begin{aligned} Q_v &= \dot{m}_v \cdot \Delta h \\ &= 2.387 \times 10^{-5}\,\text{kg/s} \cdot 2260\,\text{kJ/kgK} = 53.95\,\text{W} \end{aligned} \tag{6.4}$$

For both air and steam flow components, we need to ensure the flow rates and energy requirements match the calculated values under the most demanding conditions.

To prevent excessive pressure drops in various components, a maximum fluid speed of 3 m/s has been set as a design condition.

The density of moist air at 80°C and $100 kPa$:

With the value of the density of the moisture air, it is possible to find the components sizing of the circuit, such as the cross-section A of the pipe, through the volumetric mass flow rate, $\dot{V}$:

$$\dot{V} = \frac{\dot{m}}{\rho} \tag{6.5}$$

$$A = \frac{\dot{V}}{v} \tag{6.6}$$

Summarising the values in the below table 6.1:

Table 6.1: Value of sizing components

fluid	$\dot{m} \cdot 10^5$ [kg/s]	$\dot{V} \cdot 10^5$ $[m^3/s]$	$A \cdot 10^5 [m^2]$
1a	4.333	3.659	1.219
3ha	6.720	7.934	2.645
1w	2.387	3.99	1.33

Therefore, With this constraint, the minimum cross-section area required for the airline after mixing with steam, assuming a uniform speed distribution, is $0.265\,cm^2$.

Chapter 7

Fabrication

7.1 How it was assembled

7.1.0.1

Assembly Logbook

November

First Week:

This week, I began assembling the components for the air treatment system. Initially, everything seemed to be in place, but I had to program the PID-controlled resistance to heat the air to the desired temperature before the mixing chamber.

Second Week:

I started programming the PID controller with Arduino. Although I initially considered using LabView, a software program known for its ability to handle complex sensor data, I found it too complicated due to the different communication protocols (SPI and I2C) required by the various sensors. Consequently, I prioritised using Arduino, hoping to return to LabView if time allowed at the end of the project.

Third Week:

I studied Arduino, the sensors, and the components I could use, such as MOSFETs, TRIACs, and auto-TRIACs. After some research, I concluded that TRIACs and auto-TRIACs were the most suitable. I focused on how to control the resistance using a PID that directly regulates the temperature of the thermocouple after the resistance, setting it to 60°C.

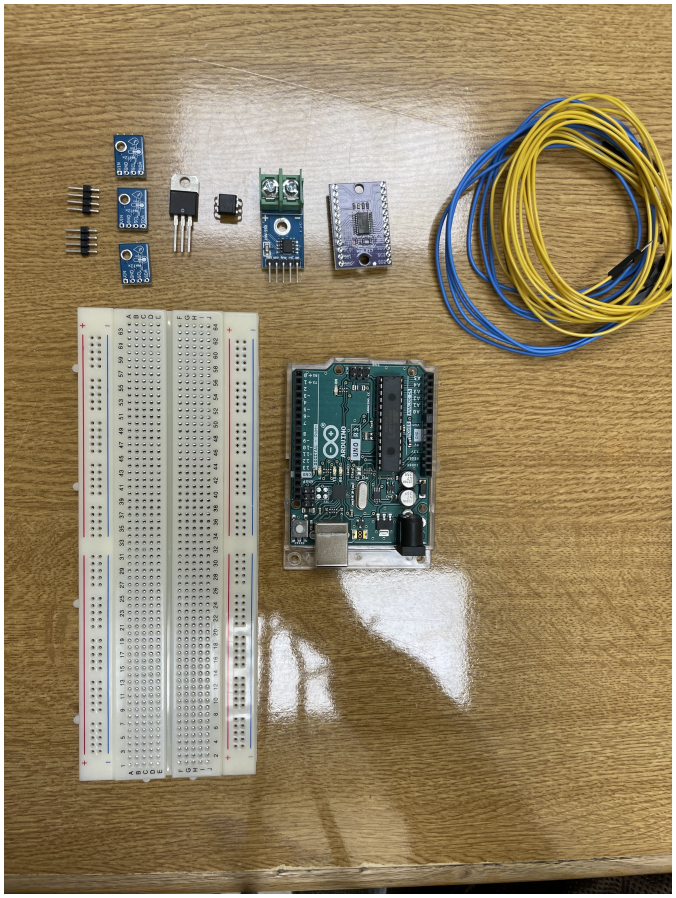

Figure 7.1: Componets

Fourth Week:

In terms of the electrical part, I encountered issues with the sensor configuration. Initially, I used multiple AHT21 sensors to measure temperature and humidity at various points in the circuit, requiring a multiplexer. However, this setup was incompatible with the PID program developed with Arduino IDE.

December

First Week:

To resolve this, I reconfigured the system to use MAX6675 sensors for temperature measurements and a single AHT21 sensor at the end of the circuit. This change simplified the system and improved compatibility with the Arduino PID program.

Second Week:

The first circuit was built:

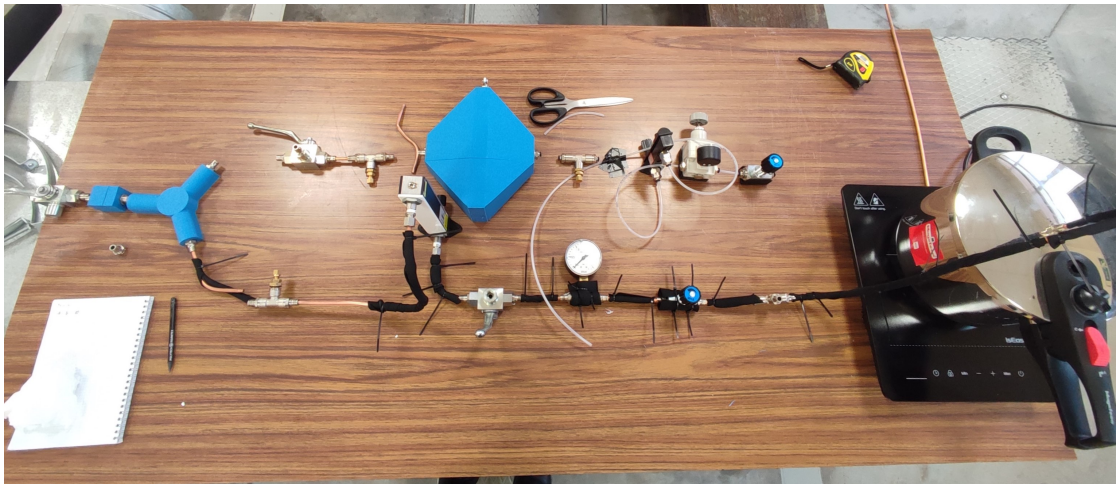

Figure 7.2: Circuit 1

Third Week:

When testing the circuit, I realised that the long time required for the thermocouple to reach 60°C caused the resistance to reach extremely high temperatures, which could melt the ABS casing 7.7. I decided to add a thermocouple wrapped around the resistance to regulate the PID based on this temperature, ensuring that the air temperature before mixing with the vapour was controlled effectively.

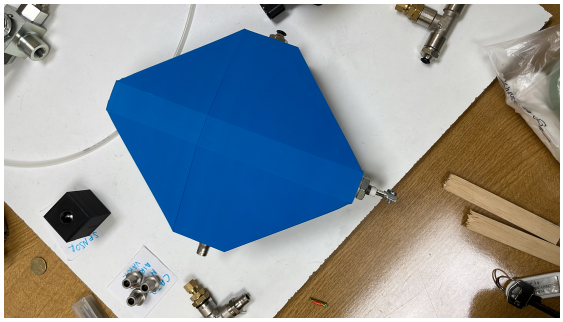

Figure 7.3: ABS resistance box

January

Second Week:

This week was spent testing different circuit configurations, arriving to the one shown in figure 7.4 and in the diagram 7.5. Each test was lengthy, requiring the circuit to reach the desired temperature, pass air and vapour, check for leaks, allow the circuit to cool, and then seal any leaks before retesting.

Third Week:

I encountered numerous problems that slowed down the work. After assembling the circuit for the first time, I realised that it was necessary to insulate the entire circuit with neoprene to prevent heat loss.

Fourth week:

Once I achieved a satisfactory configuration for the air circuit, I moved on to the vapour circuit. Initial tests showed that condensation was a major issue. I attempted to solve the condensation problem by connecting the hot air circuit to the vapour circuit to heat the vapour components, as shown in figure 7.4 and in the diagram in Figure 7.5.

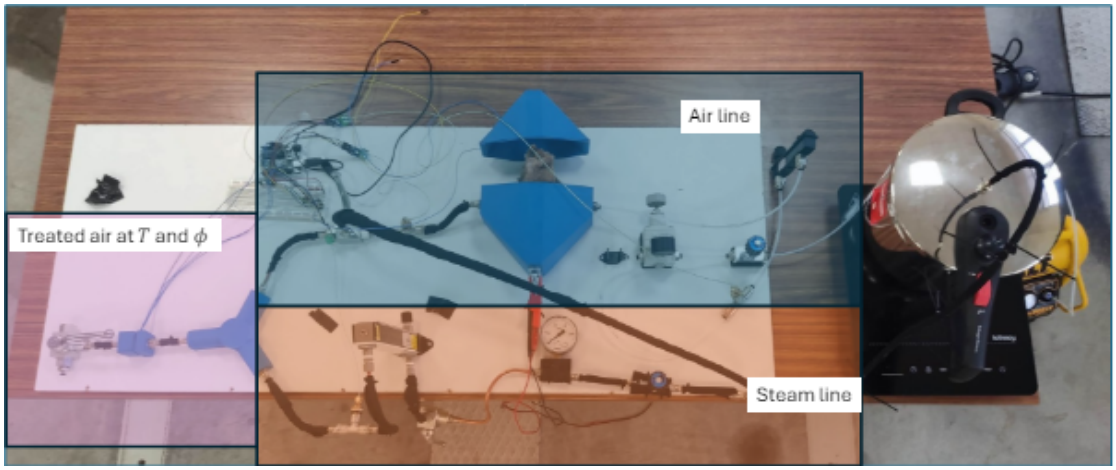

Figure 7.4: Circuit 2

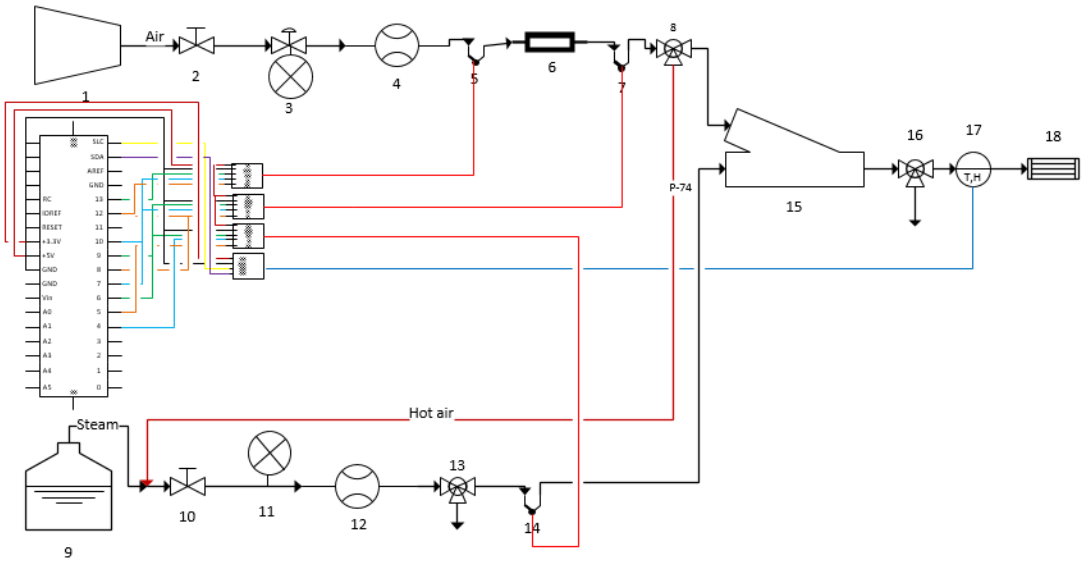

Figure 7.5: P&ID Circuit 2

February

First week:

Despite insulating with neoprene, this solution was insufficient due to significant heat losses. The air temperature dropped significantly, and the vapour circuit components did not reach the desired temperature. The resistance could reach up to 180°C, before melting, but the air temperature in the vapour circuit measured only 30°C without neoprene after travelling through the copper tube, and 40°C with it A new configuration was studied, involving the use of a three-way valve to allow vapour to pass through the circuit, heating it and eliminating possible condensation. However, closing the three-way valve caused the vapour to pass through the flowmeter, leading to condensation again.

Second week:

The first two ABS-printed casings melted 7.6, so I tried different designs for the resistance casing.

Figure 7.6: Melted boxes

Third Week:

After several trials, I determined that the ABS material was unsuitable due to its low melting point. I designed a new model using a steel cylinder for the casing, ensuring durability against high temperatures. The steel cylinder was capped with 3D-printed ABS end caps to facilitate the insertion of fittings for integration into the circuit.

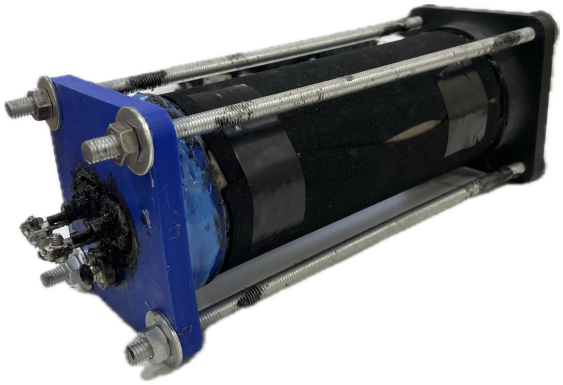

Figure 7.7: Steel resistance box

Fourth Week:

I continued to refine the circuit, ensuring that the air and vapour circuits were functioning correctly. The use of an infrared lamp to heat the flowmeter directly was considered, but it proved ineffective.

March

First week:

A new approach was taken by wrapping a constant-power heating cable around the entire vapour section to heat it directly through conduction. However, the plastic flowmeter could not be wrapped with the heating cable, so neoprene was used to insulate the flowmeter, but with limited success.

Figure 7.8: Flowmeter with neoprene

Second week:

I tried incorporating a system to absorb excess water using a vertical container with a sponge inside. Tests with containers made of plastic, 3D-printed material, and ceramic were all unsuccessful.

Figure 7.9: Systems with sponge inside

Third Week:

I realised the problem lay in the order of the components. Initially, the flowmeter was placed before the mixing chamber for air and vapour, leading to inefficiencies and losses. I decided to remove the flowmeter from the circuit and regulate the vapour flow directly with a valve.

Fourth Week:

This new configuration proved to be more effective, and the circuit began to function correctly. However, it was essential to maintain vapour humidity below 95% to prevent slight condensation, which could short-circuit the AHT21 sensor and shut down the entire Arduino circuit.

April

First week:

After stabilise the configuration, I re-insert the flowmeter at the end of the circuit, as shown in the diagram 7.10

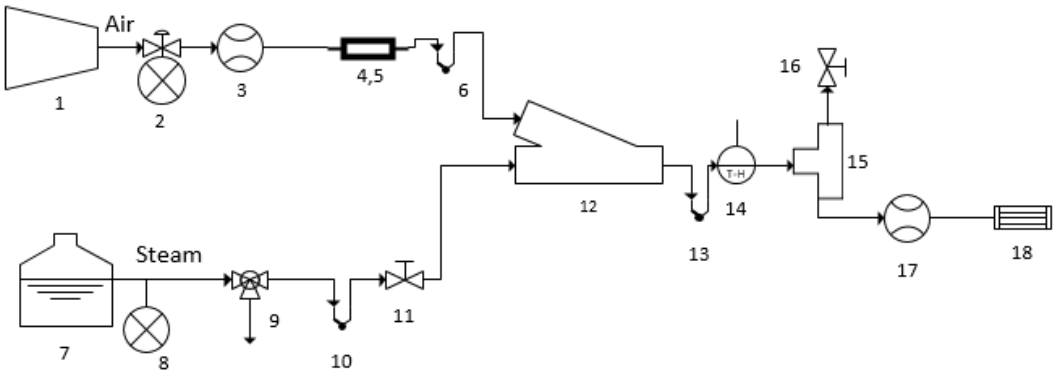

Figure 7.10: Circuit Scheme

Second week:

Despite these improvements, I found that the system was still prone to issues. The AHT21 sensor, when exposed to high humidity, caused the Arduino circuit to shut down.

Third week:

I placed the ATH21 sensor after the flower to measure the real humidity in the fuel cell, and by heating the flowmeter with the infrared lamp, it avoids condensation in the flowmeter and allows the correct measurement of temperature and humidity at the end of the circuit. The new configuration is illustrated in figure 7.11

June

First week:

After several weeks of work, the circuit was functional but still had issues with high humidity affecting the sensors. Continued efforts to improve sensor reliability and ensure stable operation of the system.

The project demonstrated significant progress in managing air and vapour circuits effectively but highlighted the need for better sensor technology for long-term stability.

7.2 The problems faced and its solutions

Summarising, several issues arose during the assembly and testing of the circuit:

- **Material for resistance casing**: The original ABS casing melted upon contact with the high-temperature resistance. This led to the decision to use a steel cylinder with ABS end caps.

- **Condensation issue**: A significant problem was the condensation of vapour in the circuit. This affected the system's performance and posed a risk to the fuel cell.

- **Heating and insulation challenges**

- **Component placement**: The initial configuration placed the flowmeter before the mixing chamber for air and vapour, resulting in various inefficiencies and losses. Removing the flowmeter and regulating vapour flow directly with a valve improved the circuit's functionality.

- **Sensor configuration**: Using multiple AHT21 sensors required a multiplexer, which was incompatible with the PID program developed with Arduino IDE. This led to a reconfiguration of the system to use MAX6675 sensors for temperature measurements and a single AHT21 sensor for humidity measurement at the end of the circuit.

For future work, the possibility of using a wet bulb temperature sensor instead of a humidity sensor should be considered. In theory, a wet bulb temperature sensor is more robust for operation at high humidity levels, as it is less likely to malfunction or shut off compared to a dedicated humidity sensor.

7.3 The assembled product

The final assembled product, shown in Figures **??** is a robust and efficient system that manages temperature and humidity, ensuring reliable performance and accurate measurements. The steel cylinder casing for the resistance, the optimised sensor configuration, and the reconfigured circuit layout all contribute to the system's success.

This system can now introduce a mixture of air and vapour into the fuel cell without the risk of flooding, thanks to the precise control of vapour flow and humidity levels. The modifications and iterations during the assembly process have resulted in a well-functioning and reliable setup.

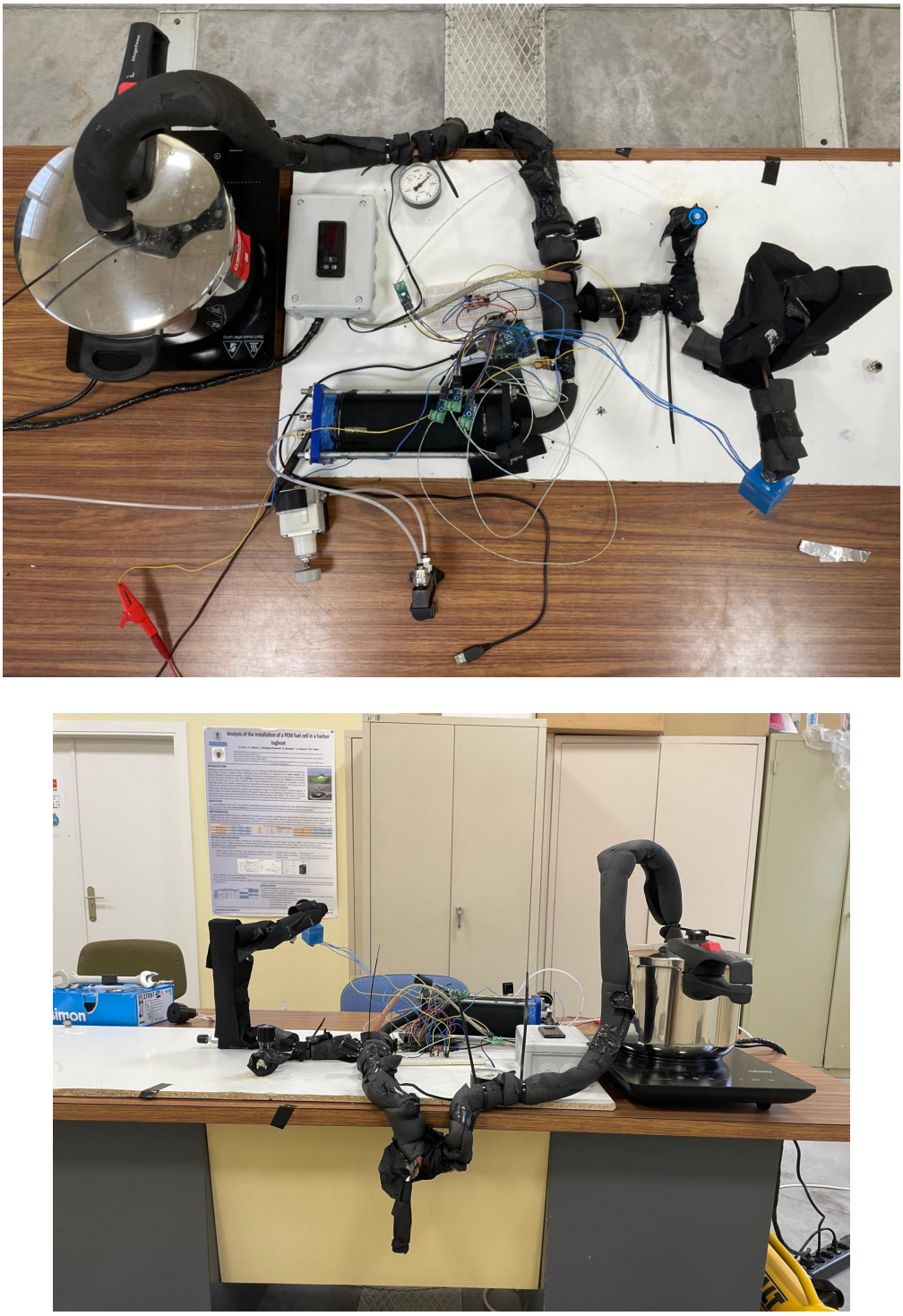

Figure 7.11: Last Circuit

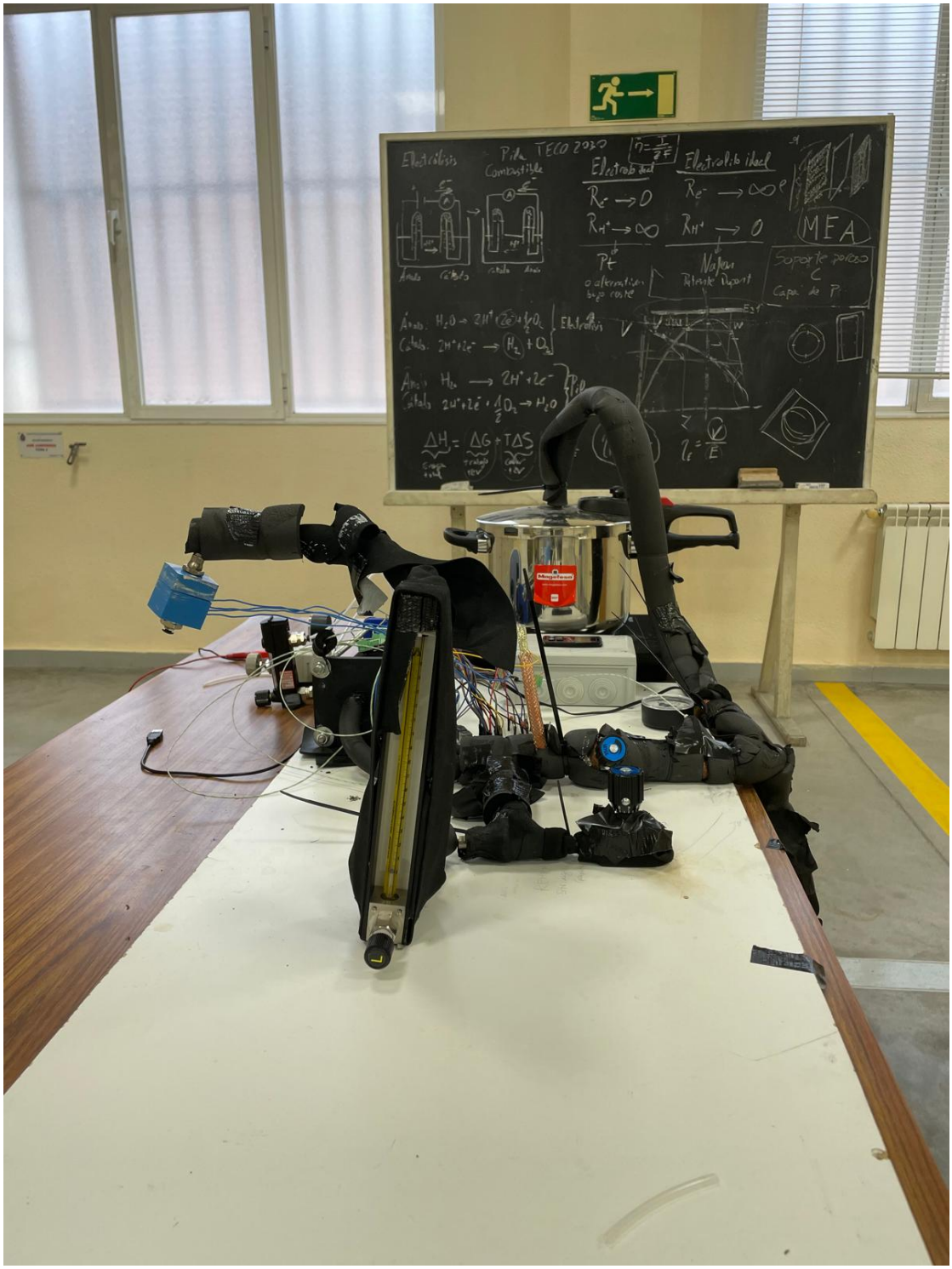

Figure 7.12: Last circuit (cont.)

Chapter 8

Conclusion

In conclusion, this thesis has successfully addressed significant challenges in designing and manufacturing the cathode air compression and treatment system for a test bench of direct methanol fuel cells. The project's primary goal was to develop an efficient air treatment system that could accurately control air temperature, humidity, and flow rate, ensuring optimal conditions for testing fuel cells. Throughout the project, various configurations were evaluated, with the final design proving robust and efficient.

The development process was marked by numerous iterations and modifications, each contributing to the refinement and improvement of the system. Challenges such as achieving the desired temperature and humidity levels were met through careful application of psychrometric principles and equations, as well as innovative engineering solutions. The ability to manage these air properties accurately is essential for studying fuel cell performance under conditions that closely mimic real-world scenarios.

The results of this work not only provide a novel approach to air treatment systems for fuel cell test benches but also fill a critical gap in the integration of renewable energy technologies. By enhancing our understanding of fuel cell behaviour and identifying ways to improve their efficiency, durability, and cost-effectiveness, this research supports the broader goal of transitioning to sustainable energy sources.

The insights gained from this thesis have practical implications for the ongoing development and optimisation of fuel cell systems. As the world grapples with climate change and the need for cleaner energy, the advancements presented in this work offer a valuable contribution to the field. Future research can build upon these findings to further enhance fuel cell technology, ultimately aiding in the global effort to reduce environmental impacts and promote a more sustainable energy future.

Appendix A

Arduino IDE

```
#include <Wire.h>
#include <Adafruit_AHTX0.h>
#include <max6675.h>

Adafruit_AHTX0 aht;

//Pin MAX6675 1
#define MAX6675_CS_1 10
#define MAX6675_SO_1 12
#define MAX6675_SCK_1 13

//Pin MAX6675 2
#define MAX6675_CS_2 7
#define MAX6675_SO_2 8
#define MAX6675_SCK_2 9

//Pin MAX6675 3
#define MAX6675_CS_3 4
#define MAX6675_SO_3 5
#define MAX6675_SCK_3 6

MAX6675 thermocouple_1(MAX6675_SCK_1, MAX6675_CS_1, MAX6675_SO_1);
MAX6675 thermocouple_2(MAX6675_SCK_2, MAX6675_CS_2, MAX6675_SO_2);
MAX6675 thermocouple_3(MAX6675_SCK_3, MAX6675_CS_3, MAX6675_SO_3);


//I/O
int PWM_pin = 3;


//Variables
```

```
32 //Cycle to read and update temperature
33 float set_temperature = 60;          //Default temperature setpoint.
34 float PID_error = 0;
35 float previous_error = 0;
36 float elapsedTime, Time, timePrev;
37 float PID_value = 0;
38
39 //PID constants
40 ////////////////////////////////////////////////////////////
41 int kp = 90;  //kp Questo parametro determina quanto forte è la
       reazione all'errore attuale: alto fa sì che il sistema reagisca
       rapidamente, ma può causare oscillazioni o sovra-escursioni (
       overshoot
42
43 int ki = 30; //ki Questo parametro aiuta a eliminare l'errore residuo
        sommando gli errori passati nel tempo: alto può portare a
       instabilità e oscillazioni persistent.
44
45 int kd = 80; //kd Questo parametro reagisce alla velocità di
       cambiamento dell'errore, tentando di prevenire sovra-escursioni e
       smorzando l'oscillazione: alto può rendere il sistema troppo cauto
        o lento a reagire.
46 ////////////////////////////////////////////////////////////
47
48
49 int PID_p = 0;    int PID_i = 0;    int PID_d = 0;
50 float last_kp = 0;
51 float last_ki = 0;
52 float last_kd = 0;
53 int PID_values_fixed =0;
54
55 //Configurazione del PWM per il segnale al MOSFET, del AHT21 e del
       MAX6675
56 void setup() {
57   Serial.begin(9600);
58
59   Serial.println("MAX6675 test");
60   // wait for MAX chip to stabilize
61   delay(1000);
62
63   {
64   Serial.begin(9600);
65   Serial.println("Adafruit AHT10/AHT20 demo!");
66
67   if (! aht.begin()) {
68     Serial.println("Could not find AHT? Check wiring");
69     while (1) delay(10);
70   }
71   Serial.println("AHT10 or AHT20 found");
```

```
72 }
73  pinMode(PWM_pin,OUTPUT);
74  TCCR2B = TCCR2B & B11111000 | 0x03;   //pin 3 e 11 frequenza PWM di
      928.5 Hz (MI SA CHE è 980 Hz)
75  Time = millis();
76
77 }
78
79 void loop() {
80   // Basic readout test for sensor 1
81    Serial.print("Sensor 1 - Celsius: ");
82    Serial.println(thermocouple_1.readCelsius());
83
84    // Basic readout test for sensor 2
85   Serial.print("Sensor 2 - Celsius: ");
86   Serial.println(thermocouple_2.readCelsius());
87
88   // Basic readout test for sensor 3
89   Serial.print("Sensor 3 - Celsius: ");
90   Serial.println(thermocouple_3.readCelsius());
91
92 // Read AHT21 sensor data
93   sensors_event_t humidity, temp;
94   aht.getEvent(&humidity, &temp);// populate temp and humidity
      objects with fresh data
95   Serial.print("Temperature: "); Serial.print(temp.temperature);
      Serial.println(" degrees C");
96   Serial.print("Humidity: "); Serial.print(humidity.relative_humidity
      ); Serial.println("% rH");
97
98 //Next we calculate the error between the setpoint and the real value
      of sensor 2
99   PID_error = set_temperature - thermocouple_2.readCelsius() + 3;  //
      +3 NECESSARIO????
100  //Calculate the P value
101  PID_p = 0.01*kp * PID_error;
102  //Calculate the I value in a range on +-3
103  PID_i = 0.01*PID_i + (ki * PID_error);
104
105  //For derivative we need real time to calculate speed change rate
106  timePrev = Time;                            // the previous time is
       stored before the actual time read
107  Time = millis();                            // actual time read
108  elapsedTime = (Time - timePrev) / 1000;     //calcola il tempo
      trascorso (o 'elapsed time') tra le due letture del tempo in
      secondi
109
110  //Now we can calculate the D calue
111  PID_d = 0.01*kd*((PID_error - previous_error)/elapsedTime);
```

```
112   //Final total PID value is the sum of P + I + D
113   PID_value = PID_p + PID_i + PID_d;  //Un valore PID più alto
        corrisponde a una maggiore potenza della resistenza
114
115   //We define PWM range between 0 and 255
116   PID_value = constrain(PID_value, 0, 255);
117   Serial.println(PID_value);
118   //Now we can write the PWM signal to the mosfet on digital pin D3
119   //Since we activate the MOSFET with a 0 to the base of the BJT, we
        write 255-PID value (inverted)
120   analogWrite(PWM_pin, PID_value);
121   previous_error = PID_error;     //Remember to store the previous
        error for next loop.
122   delay(1000);
123
124 }
```

Bibliography

[1] ExxonMobil. *Energy demand: Three drivers*. 2024. URL: https://corporate.exxonmobil.com/what-we-do/energy-supply/global-outlook/energy-demand#Industrial (cit. on p. 1).

[2] United Nations Environment Programme. *The sectoral solution to climate change.* 2023. URL: https://www.unep.org/interactive/sectoral-solution-climate-change/ (cit. on p. 1).

[3] United Nations. *Fossils fuels at the heart of the planetary environmental crisis: UN experts*. 2023. URL: https://www.ohchr.org/en/press-releases/2023/11/fossils-fuels-heart-planetary-environmental-crisis-un-experts (cit. on p. 1).

[4] Statista. *Global share of CO2 emissions from fossil fuel and cement production as of 2019*. Accessed on October 2, 2023. 2021. URL: https://www.statista.com/statistics/1129656/global-share-of-co2-emissions-from-fossil-fuel-and-cement/ (cit. on p. 1).

[5] BEN SHRAGER. *Energy Storage Innovation to Combat Climate Change*. 2023. URL: https://www.energy.gov/oe/articles/energy-storage-innovation-combat-climate-change (cit. on p. 2).

[6] Panoucontrol. *Sustainable Energy Storage Solutions: A Key to Combating Climate Change and Protecting the Environment*. 2023. URL: https://primebatteries.com/sustainable-energy-storage-solutions/ (cit. on p. 2).

[7] Massimo Santarelli. *DESCRIZIONE GENERALE DELLA CELLA E DEI SUOI PRINCIPI DI FUNZIONAMENTO* (cit. on pp. 2, 13).

[8] Myrtle Cory Jefferson. *Fuel cell primer presented to Ridgefield High School*. URL: https://slideplayer.com/slide/12677630/ (cit. on p. 3).

[9] U.S. Department of Energy. *Fuel Cells*. URL: https://www.energy.gov/eere/fuelcells/fuel-cells (cit. on p. 4).

[10] David A. J. Rand Andrew L. Dicks. *Fuel Cell Systems Explained*. Whiley, 2018 (cit. on p. 5).

[11] Jee-Hoon Jung and Shehab Ahmed. «Dynamic Model of PEM Fuel Cell Using Real-time Simulation Techniques». In: (2010). URL: https://www.researchgate.net/publication/263991127_Dynamic_Model_of_PEM_Fuel_Cell_Using_Real-time_Simulation_Techniques (cit. on p. 6).

[12] Methanex Corporation. *How Methanol is Produced*. 2024. URL: https://www.methanex.com/about-methanol/how-methanol-is-produced/ (cit. on p. 7).

[13] Utsav Saxena Sarthak Tibdewal and Anand V. P. Gurumoorthy. «Hydrogen economy vs. Methanol economy». In: (2014). URL: https://www.researchgate.net/publication/277005223_Hydrogen_economy_vs_Methanol_economy (cit. on p. 9).

[14] Vladimir Meca, Oscar Santiago, Elena Posada, Rafael d'Amore-Domenech, Antonio Villalba-Herreros, and T.J. Leo. «Anode Flow Field Design Effect on Direct Methanol Fuel Cells». In: Jan. 2023, pp. 1034–1040. DOI: 10.52202/069564-0094 (cit. on p. 10).

[15] Gregor Hoogers. *FUEL CELL TECHNOLOGY HANDBOOK*. CRC Press, 2003 (cit. on pp. 11, 19).

[16] et al Wei Wuen Ng Hui San Thiam. «A State-of-Art on the Development of Nafion-Based Membrane for Performance Improvement in Direct Methanol Fuel Cells». In: (2022). URL: https://www.mdpi.com/2077-0375/12/5/506 (cit. on p. 12).

[17] Kingshuk Dutta, ed. *Direct Methanol Fuel Cell Technology*. 2020. DOI: https://doi.org/10.1016/C2018-0-04199-7 (cit. on p. 12).

[18] Andrew L. Dicks and David A. J. Rand. *Fuel Cell Systems Explained*. Whiley, 2018 (cit. on p. 14).

[19] V.M. Barragán A. Heinzel. «A review of the state-of-the-art of the methanol crossover in direct methanol fuel cells». In: (1999). URL: https://www.sciencedirect.com/science/article/pii/S037877539900302X (cit. on p. 14).

[20] R. Gültekin Akay et al Erce Şengül Hülya Erdener. «Effects of sulfonated polyether-etherketone (SPEEK) and composite membranes on the proton exchange membrane fuel cell (PEMFC) performance». In: (2009). URL: https://www.sciencedirect.com/science/article/pii/S0360319908011270?via%3Dihub (cit. on p. 15).

[21] Andreas Glüsen C. Ozgur Colpan David Ouellette. «Reduction of methanol crossover in a flowing electrolyte-direct methanol fuel cell». In: (2017). URL: https://www.sciencedirect.com/science/article/pii/S0360319917300241 (cit. on p. 16).

[22] Bing Fu Feifan Wang. «Anion-exchange membranes for direct methanol alkaline fuel cells». In: (2020). URL: https://doi.org/10.1016/b978-0-12-819158-3.00004-5 (cit. on p. 17).

[23] G. Vlachogiannopoulos K. Scott E. Yu. «Performance of a direct methanol alkaline membrane fuel cell». In: (2007). URL: https://www.sciencedirect.com/science/article/pii/S0378775307018794 (cit. on p. 17).

[24] Hubert A. Gasteiger, Nenad M. Markovic, Jr. Ross Philip N., and Elton J. Cairns. «CO Electrooxidation on Well-Characterized Pt-Ru Alloys». In: *The Journal of Physical Chemistry* (1994). DOI: 10.1021/j100053a042 (cit. on p. 18).

[25] Marcos Mandado Ana S. Moura José L. C. Fajín and Maria Natália D. S. Cordeiro. «Ruthenium–Platinum Catalysts and Direct Methanol Fuel Cells (DMFC): A Review of Theoretical and Experimental Breakthroughs». In: (2017). URL: https://www.mdpi.com/2073-4344/7/2/47 (cit. on p. 18).

[26] William D. King, James D. Corn, Oliver J. Murphy, Deborah L. Boxall, Edward A. Kenik, Krzysztof C. Kwiatkowski, Stuart R. Stock, and C. M. Lukehart. «Pt-Ru and Pt-Ru-P/Carbon Nanocomposites: Synthesis, Characterization, and Unexpected Performance as Direct Methanol Fuel Cell (DMFC) Anode Catalysts». In: *The Journal of Physical Chemistry B* 107.23 (2003), pp. 5465–5473. DOI: 10.1021/jp0300521 (cit. on p. 18).

[27] G. Álvarez et al J.R.C. Salgado F. Alcaide. «Pt–Ru electrocatalysts supported on ordered mesoporous carbon for direct methanol fuel cell». In: (2009). DOI: 10.1016/j.jpowsour.2009.01.002 (cit. on p. 18).

[28] A. Schmitz et al A. Oedegaard C. Hebling. «Influence of diffusion layer properties on low-temperature DMFC». In: *Journal of Power Sources* (1994). URL: https://www.sciencedirect.com/science/article/pii/S0378775303009510?via%3Dihub (cit. on pp. 18, 19).

[29] Bhagyalakhi Baruah and Pritam Deb. «Performance and application of carbon-based electrocatalysts in direct methanol fuel cell». In: (2021). URL: https://pubs.rsc.org/en/content/articlehtml/2021/ma/d1ma00503k (cit. on p. 19).

[30] Wai Yin Wong et al Shuaiba Samad Kee Shyuan Loh. «Carbon and non-carbon support materials for platinum-based catalysts in fuel cells». In: *International Journal of Hydrogen Energy* (2018). URL: https://www.sciencedirect.com/science/article/pii/S0360319918306578 (cit. on p. 19).

[31] Jason Morgan. *Study of Gas Diffusion Layers in direct methanol fuel cells (DMFC)*. 2008. URL: https://scholars.unh.edu/cgi/viewcontent.cgi?article=1367&context=thesis (cit. on p. 19).

[32] Fuel Cell Store. *Gas diffusion layers*. URL: https://fuelcellstore.com/fuel-cell-components/gas-diffusion-layers (cit. on p. 19).

[33] Colleen Spiegel. *Low-Temperature Bipolar Plates*. 2017. URL: https://www.fuelcellstore.com/blog-section/low-temperature-bipolar-plates (cit. on p. 20).

[34] Runjing Xu Xin Gao Jiayi Chen. «Research progress and prospect of the materials of bipolar plates for proton exchange membrane fuel cells (PEMFCs)». In: (2023). URL: https://www.sciencedirect.com/science/article/pii/S0360319923045688?via%3Dihub (cit. on p. 20).

[35] Leonard Bonville Aubrey Tang Louis Crisci. «An overview of bipolar plates in proton exchange membrane fuel cells». In: (2021). URL: https://doi.org/10.1063/5.0031447 (cit. on p. 20).

[36] Xianguo Li. «Bipolar plates and flow field design». In: (2023). URL: https://doi.org/10.1016/B978-0-323-99485-9.00003-4 (cit. on pp. 22, 23).

[37] Giosuè Giacoppo Orazio Barbera. *Direct Methanol Fuel Cell Technology*. Kingshuk Dutta, 2020. DOI: https://doi.org/10.1016/C2018-0-04199-7 (cit. on p. 22).

[38] et al. Jinshi Wang Junjie Yan. «On Flow Maldistribution in PEMFC Stacks». In: (2011). URL: https://www.researchgate.net/publication/232875888_On_flow_maldistribution_in_PEMFC_stacks (cit. on p. 22).

[39] Mohammad Bakhshi-Jooybari Moosa Balali Osia Seyed Jamal Hosseinipour and Abdolhamid Gorgi. «Forming Metallic Micro-Feature Bipolar Plates for Fuel CellUsing Combined Hydroforming and Stamping Processes». In: (2013). URL: https://www.researchgate.net/publication/272850184_Forming_Metallic_Micro-Feature_Bipolar_Plates_for_Fuel_Cell_Using_Combined_Hydroforming_and_Stamping_Processes (cit. on p. 23).

[40] W.R.W. Daud S.K. Kamarudin F. Achmad. «Overview on the application of direct methanol fuel cell (DMFC) for portable electronic devices». In: (2009). URL: https://doi.org/10.1016/j.ijhydene.2009.06.013 (cit. on p. 25).

[41] et al. Detlef Gunther Mainz-Kastel. «AIR HUMIDIFICATION FOR FUEL CELL APPLICATIONS». In: (2006). pdf. URL: https://patentimages.storage.googleapis.com/9c/3e/aa/2ad23881e2ac14/US20060134482A1.pdf (cit. on p. 26).

[42] et al. Zhiyang Liu Jian Chen. «Modeling and Control of Cathode Air Humidity for PEM Fuel Cell Systems». In: (2017). DOI: doi.org/10.1016/j.ifacol.2017.08.943 (cit. on p. 26).

[43] HYfindr0. *Fuel cell air compressors*. 2009. URL: https://hyfindr.com/en/hydrogen-knowledge/hydrogen-fuel-cell-air-compressors (cit. on p. 26).

[44] Amat. *Enhancing fuel cell performance: The four critical areas*. URL: https://www.amot.com/en/blog/enhancing-fuel-cell-performance.html (cit. on p. 27).

[45] Min Soo Kim Beom Jun Kim. «Studies on the cathode humidification by exhaust gas recirculation for PEM fuel cell». In: (2012). URL: https://doi.org/10.1016/j.ijhydene.2011.11.103 (cit. on p. 28).

[46] J.-P. Poirot-Crouvezier S. Rodosik and Y. Bultel. «Impact of humidification by cathode exhaust gases recirculation on a PEMFC system for automotive applications». In: (2019). DOI: https://doi.org/10.1016/j.ijhydene.2018.11.139 (cit. on p. 28).

[47] Howard N. Shapiro Michael J. Moran. *Fundamentals of Engineering Thermodynamics*. Whiley, 2018 (cit. on pp. 40, 42).

[48] Whiley. *PROPERTY TABLES AND CHARTS (SI UNITS)*. https://cecs.wright.edu/people/faculty/sthomas/htappendix01.pdf. 2010 (cit. on p. 40).